MÉRA Workshop Proceedings

Met Éireann
2018

Disclaimer

ISSN 1393-905X

Title: MÉRA Workshop Proceedings
Editors: Emily Gleeson, Eoin Whelan
Authors: Julian Aherne, Hazel Cathcart, Laura Cooke, João Correia, Joan de Lacy, Frédéric Dias, Eadaoin Doddy, Jason Flanagan, Graham Florence, Sarah Gallagher, Edward Graham, Seánie Griffin, Jelena Janjić, Chris Kidd, Eoin Lettice, Frank McDermott, Owen Naughton, Paul Nolan, Conor Sweeney, Christopher Werner, Kayla Wilkins

Acknowledgements: We would like to thank all of the workshop delegates and presenters for their contributions. We would also like to thank Jevon Brennan-Keane and Laura Zubiate for their assistance with this workshop.

Contents

Photo: Sinéad Duffy

Weather observations are routinely used to analyse the past climate. Climate reanalyses may also be used for this purpose. These give a numerical description of the recent climate and are produced by combining models with weather observations. They contain estimates of atmospheric parameters such as air temperature, pressure and wind at different heights above the ground, and surface parameters such as precipitation, soil moisture content and temperatures, and sea-surface temperature. Because they are carried out using a fixed version of a forecast model and a data assimilation system which utilises historical observations, they produce parameters that are physically consistent and often not routinely observed. Thus, climate reanalyses have the potential to extend the knowledge gained from current observation networks.

Over the past few years researchers at Met Éireann have produced a climate reanalysis dataset, called MÉRA - Met Éireann Reanalysis, for the period 1981-2017 for an area covering Ireland, the UK and northern France. This dataset was launched in May 2017 and currently has over 100 users in Ireland, the U.K., Germany, the Netherlands, Canada and the U.S. On May 17th 2018 we held the first workshop for users of the data. The workshop consisted of 15 very interesting talks spread across sessions on climate applications, precipitation and hydrology, energy, waves and storms. Short papers on a number of these talks are included in this workshop proceedings.

Further scientific information on MÉRA can be found in the following publications:

Gleeson, E., Whelan, E., and Hanley, J.: Met Éireann high resolution reanalysis for Ireland, Adv. Sci. Res., 14, 49-61, https://doi.org/10.5194/asr-14-49-2017, 2017.
https://www.adv-sci-res.net/14/49/2017/asr-14-49-2017.pdf

Whelan, E., E. Gleeson, and J. Hanley: An evaluation of MÉRA, a high resolution mesoscale regional reanalysis. J. Appl. Meteor. Climatol., **57**, 2179-2196, doi:10.1175/JAMC-D-17-0354.1, 2018.
https://journals.ametsoc.org/doi/abs/10.1175/JAMC-D-17-0354.1

For access to the data, please e-mail mera@met.ie.

Towards a Definitive Historical High-Resolution Climate Dataset for Ireland

Jason Flanagan[1], Paul Nolan[1]

[1]Irish Centre for High-End Computing

1 Introduction

There is a strong and constant demand from various sectors for long-term, high-resolution (both temporal and spatial), gridded climate datasets. In Ireland, such datasets have traditionally been based on station observations and are therefore subject to several shortcomings. For instance, there is a lack of representivity in regions with few observing stations whilst station data are prone to error and/or missing values. Reanalyses do not suffer from such drawbacks and represent a viable alternative to observations for the production of gridded datasets. In 2017, Met Éireann completed a 36-year simulation (MÉRA) at 2.5 km resolution for the period 1981-2016 (Gleeson et al, 2017; Whelan et al, 2018) using the shared ALADIN-HIRLAM numerical weather prediction system. The MÉRA dataset, which is stored as a series of 3-hour and 33-hour forecasts, have been archived by Met Éireann at 1-hour intervals. A full description of the available data and a selection of uncertainty estimates is given in Whelan et al. (2017) and Gleeson et al. (2017), respectively. Seperately, the Irish Centre for High-End Computing (ICHEC) has recently performed two high-resolution simulations of the Irish climate. The simulations were achieved with the Regional Climate Models COSMO-CLM5 and WRF v3.7.1 at maximum resolutions of 1.5 km and 2 km respectively. The datasets produced contain both hourly and daily outputs for an array of sub-surface, surface and atmospheric fields for the period 1981-2016. Although at lower spatial resolution than the ICHEC datasets, the MÉRA dataset has the distinct advantage of having been produced with the aid of a data assimilation component. Here, we present analyses that evaluate uncertainty estimates at various scales for several climate variables from the three model datasets and give example-appropriate skill scores. The validation results presented here form part of ongoing research aimed at the production of definitive, high-resolution, gridded Irish climate datasets for the period 1981-present.

2 Model Outputs

Several model outputs have been validated using station, gridded and satellite observations from a variety of sources. The climate variables tested include precipitation, 2 m temperature, 10 m wind speeds, relative humidity, mean sea level pressure and global irradiance.

Precipitation

Gridded datasets of observed daily (09-09 UTC) accumulated precipitation at 1 km resolution that cover the Republic of Ireland (ROI) (Walsh, 2012) and Northern Ireland (NI) (Tanguy at al., 2016) for the period 1981-2015 have been obtained from Met Éireann and the Centre for Ecology and Hydrology in the UK. An area-averaging algorithm has been applied to transform the gridded observations to each of the three model grids and to facilitate the calculation of bias, mean absolute error (MAE) and standard deviation (STD) (Table 1) and various skill scores (Table 2). With the exception of NI bias, the MÉRA dataset displays least error and variance. Similarly, for the majority of skill scores and thresholds examined, MÉRA outperforms both WRF and COSMO-CLM.

A similar uncertainty analysis has been performed utilising hourly station observations from 25 Met Éireann synoptic stations. Overall biases (found by treating all 25 time series as one time-ordered

dataset) for each model were less than 0.01 mm whilst overall MAE and STD values were 0.177 mm, 0.176 mm, 0.155 mm and 0.326 mm, 0.327 mm, 0.294 mm for COSMO-CLM, WRF and MÉRA respectively.

Table 1: 24-hour rainfall accumulation (mm) uncertainty estimates found for each model through comparison with ROI and NI (values in parentheses) gridded observation datasets.

(mm)	COSMO-CLM: ROI (NI)	WRF: ROI (NI)	MÉRA: ROI (NI)
Bias	0.182 (0.366)	0.238 (0.207)	0.094 (0.420)
MAE	4.067 (3.893)	3.241 (3.336)	2.602 (2.656)
STD	6.667 (6.317)	5.671 (5.664)	4.547 (4.493)

Table 2: A selection of 24-hour rainfall accumulation skill scores at various thresholds found for each model through comparison with ROI and NI (values in parentheses) gridded observations.

		Threshold (mm) – NI values in brackets						
Skill Score	**Model**	**0.1**	**1.0**	**5.0**	**10.0**	**20.0**	**30.0**	**50.0**
Accuracy	**COSMO-CLM**	0.91 (0.91)	0.74 (0.74)	0.73 (0.72)	0.82 (0.83)	0.94 (0.95)	0.98 (0.99)	0.997 (0.998)
	WRF	0.89 (0.90)	0.77 (0.75)	0.78 (0.76)	0.86 (0.86)	0.96 (0.96)	0.99 (0.99)	0.998 (0.999)
	MÉRA	0.89 (0.91)	0.80 (0.80)	0.83 (0.81)	0.89 (0.88)	0.96 (0.97)	0.99 (0.99)	0.998 (0.999)
Frequency Bias	**COSMO-CLM**	0.98 (0.99)	0.93 (0.97)	0.99 (1.05)	1.11 (1.18)	1.35 (1.35)	1.53 (1.56)	1.98 (2.17)
	WRF	0.99 (0.99)	0.96 (0.97)	1.03 (1.03)	1.14 (1.13)	1.30 (1.23)	1.39 (1.31)	1.58 (1.72)
	MÉRA	0.98 (1.00)	0.95 (1.02)	1.02 (1.10)	1.11 (1.21)	1.18 (1.24)	1.14 (1.18)	1.11 (1.16)
Hit Rate	**COSMO-CLM**	0.94 (0.95)	0.80 (0.81)	0.63 (0.63)	0.52 (0.50)	0.38 (0.35)	0.30 (0.36)	0.20 (0.15)
	WRF	0.94 (0.94)	0.82 (0.81)	0.68 (0.64)	0.57 (0.51)	0.42 (0.33)	0.33 (0.24)	0.21 (0.13)
	MÉRA	0.93 (0.95)	0.83 (0.86)	0.73 (0.74)	0.64 (0.63)	0.48 (0.46)	0.39 (0.35)	0.27 (0.15)
False Alarm Rate	**COSMO-CLM**	0.82 (0.84)	0.45 (0.50)	0.21 (0.23)	0.12 (0.12)	0.04 (0.03)	0.01 (0.01)	0.002 (0.001)
	WRF	0.73 (0.77)	0.34 (0.40)	0.17 (0.18)	0.09 (0.09)	0.03 (0.02)	0.01 (0.01)	0.001 (0.001)
	MÉRA	0.61 (0.69)	0.25 (0.35)	0.13 (0.16)	0.07 (0.08)	0.02 (0.02)	0.01 (0.005)	0.001 (0.001)
Hanssen-Kuiper (KSS)	**COSMO-CLM**	0.12 (0.11)	0.34 (0.32)	0.42 (0.40)	0.41 (0.38)	0.35 (0.32)	0.29 (0.25)	0.19 (0.14)
	WRF	0.21 (0.17)	0.48 (0.41)	0.51 (0.46)	0.48 (0.41)	0.39 (0.31)	0.32 (0.24)	0.21 (0.13)
	MÉRA	0.32 (0.26)	0.58 (0.52)	0.60 (0.59)	0.57 (0.55)	0.46 (0.44)	0.38 (0.34)	0.27 (0.15)
Equitable Threat (ETS)	**COSMO-CLM**	0.05 (0.05)	0.19 (0.18)	0.26 (0.25)	0.24 (0.22)	0.17 (0.16)	0.13 (0.11)	0.07 (0.05)
	WRF	0.11 (0.09)	0.30 (0.25)	0.34 (0.30)	0.29 (0.24)	0.21 (0.16)	0.16 (0.11)	0.09 (0.05)
	MÉRA	0.17 (0.15)	0.39 (0.35)	0.43 (0.40)	0.37 (0.34)	0.27 (0.25)	0.22 (0.19)	0.15 (0.07)

2 m Temperature

A similar analysis of 2 m temperature (ROI only) has been performed at hourly and daily time-scales utilising Met Éireann synoptic station and gridded observations (Table 3).
As with precipitation, MÉRA is the better performer of the three. The skill scores shown in Table 2 have also been calculated for 2 m daily mean temperature (not shown) at 6 thresholds (-5, 0, 5, 10, 25 and 20°C). The results confirm the pattern seen in Table 3 with MÉRA showing greater skill for the majority of score and thresholds tested.

Table 3: Overall hourly and daily mean (in parentheses) 2m temperature (°C) uncertainty estimates found through comparison with Met Éireann synoptic station and (ROI only) gridded observations.

(°C)	COSMO-CLM	WRF	MÉRA
Bias	-0.18 (-0.36)	-0.30 (-0.63)	-0.11 (-0.38)
MAE	1.33 (1.19)	1.30 (1.18)	0.81 (0.89)
STD	1.19 (1.49)	1.33 (1.33)	0.91 (1.04)

10 m Winds

Hourly time series of 10 m wind speeds from 23 Met Éireann synoptic stations – winds are not measured at the Markree and Phoenix Park stations – have been compared to each of the 3 model outputs. The MÉRA dataset has lowest MAE and STD at 17 and 22 of the 23 stations, respectively. A summary (where all 23 station time series are treated as a single dataset) is given in Table 4.

Table 4: Overall hourly 10 m wind speed (m/s) uncertainty estimates for each model through comparison with 23 Met Éireann synoptic station time series.

(m/s)	COSMO-CLM	WRF	MÉRA
Bias	0.85	0.07	0.29
MAE	1.89	1.67	1.27
STD	2.30	2.24	1.65

Relative Humidity

Hourly time series from 24 Met Éireann synoptic stations have been used to determine relative humidity uncertainty estimates (including percentage errors PE (and their standard deviations) and correlations). Data from Sherkin Island were excluded from this analysis due to the appearance of several multi-week periods of spurious measurements within the time series. MÉRA out-performs both COSMO-CLM and WRF at each station. Table 5 summarises the (overall) results found.

Table 5: Overall hourly relative humidity (%) uncertainty estimates (plus correlations) found through comparison with time series from 24 Met Éireann synoptic stations.

(%)	COSMO-CLM	WRF	MÉRA
Bias (STD)	-2.86 (5.85)	0.95 (6.61)	-0.42 (3.59)
MAE (STD)	7.58 (3.53)	7.67 (3.93)	5.47 (2.19)
PE (STD)	-2.75 (7.64)	2.16 (8.92)	-0.04 (4.72)
| PE | (STD)	9.39 (4.94)	9.83 (6.08)	6.89 (3.33)
Correlation	0.66	0.57	0.80

Mean Sea Level Pressure

Mean sea level pressure uncertainty estimates and correlations have been determined for all 25 Met Éireann synoptic stations. The MÉRA dataset shows lowest MAE and STD and highest correlation at all stations (not shown). A summary of the results found is given in Table 6.

Table 6: As in Table 5 but for mean sea level pressure (hPa) at 25 Met Éireann synoptic stations.

(hPa)	COSMO-CLM	WRF	MÉRA
Bias (STD)	-0.87 (2.56)	-0.20 (2.39)	0.03 (0.51)
MAE (STD)	1.96 (1.87)	1.69 (1.70)	0.37 (0.36)
PE (STD)	-0.09 (0.25)	-0.02 (0.24)	0.003 (0.05)

| PE | (STD)	0.19 (0.19)	0.17 (0.17)	0.04 (0.04)
Correlation	0.98	0.98	1

Global Irradiance

Both satellite and station data have been used to determine hourly, daily and annual average global irradiance (GI) uncertainty estimates. The average annual (1998-2011, only) and hourly (Oct. 2010 – Dec. 2015, only) satellite datasets were obtained from the Photovoltaic Geographical Information System (PVGIS) (Huld et al., 2012) and EUMETSAT, respectively, whilst the daily data were obtained from 18 Met Éireann stations. A summary of the results are given in Tables 7-9. At each timescale, MÉRA has the lowest error – the daily analysis has been performed for COSMO-CLM and MÉRA only.

Table 7: Hourly GI uncertainty estimates (kWh/m^2) found through comparison with EUMETSAT 10/2010 – 12/2015 satellite data.

(kWh/m^2)	**COSMO-CLM**	**WRF**	**MÉRA**
Bias	0.008	0.079	-0.003
MAE	0.103	0.127	0.086
STD	0.094	0.113	0.088

Table 8: Overall daily GI uncertainty estimates (MJ/m^2) found through comparison with observations from 18 Met Éireann stations.

(MJ/m^2)	**COSMO-CLM**	**MÉRA**
Bias	0.167	0.122
MAE	0.809	0.589
STD	1.189	0.855

Table 9: Average annual GI uncertainty estimates (expressed as a percentage) found through comparison with PVGIS 1998-2011 satellite data.

(%)	**COSMO-CLM**	**WRF**	**MÉRA**
Bias	2.83	29.17	-0.81
MAE	3.58	29.17	3.48
STD	3.47	4.76	4.46

3 References

Gleeson, E., Whelan, E., and Hanley, J.: Met Éireann high resolution reanalysis for Ireland, Adv. Sci. Res., 14, 49–61, doi:10.5194/asr-14-49-2017, 2017.

Huld T., Müller R. and Gambardella A.: "A new solar radiation database for estimating PV performance in Europe and Africa". Solar Energy, 86, 1803-1815, 2012.

Tanguy, M.; Dixon, H.; Prosdocimi, I.; Morris, D. G.; Keller, V. D. J.: Gridded estimates of daily and monthly areal rainfall for the United Kingdom (1890-2015) [CEH-GEAR]. NERC Environmental Information Data Centre. https://doi.org/10.5285/33604ea0-c238-4488-813d-0ad9ab7c51ca, 2016.

Walsh, S.: 'A Summary of Climate Averages for Ireland 1981–2010', [report], Met Éireann, 14, *Climatological Note*, 14, 2012.

Whelan, E., E. Gleeson, and J. Hanley: An evaluation of MÉRA, a high resolution mesoscale regional reanalysis. J. Appl. Meteor. Climatol., In press, https://doi.org/10.1175/JAMC-D-17-0354.1, 2018.

Whelan, E., Hanley, J. and Gleeson, E.: 'The MÉRA Data Archive', [report], Met Éireann, 2017-08-04, Met Éireann Technical Note, 65, 2017.

High-Resolution Gridded Datasets of Hydroclimate Indices for Ireland

Christopher Werner[1], Paul Nolan[1], Owen Naughton[2]

[1]Irish Centre for High-End Computing
[2]Trinity College Dublin

1 Introduction

There is constant demand from industry, research and government agencies for high quality, long-term, gridded datasets of hydroclimatic variables for conducting climate research. These have applications in a wide variety of fields such as agriculture, hydrology, public health, energy, planning and studies in observed climate change trends and vulnerability. Variables such as evapotranspiration and soil moisture conditions are crucial in ensuring water sustainability, monitoring groundwater recharge, agronomic management and the management of flood and drought risk. Numerical weather prediction (NWP) models, can be used to reanalyse historic weather conditions and produce spatially and temporally homogeneous, multi-decadal gridded datasets. This article describes the application of three NWP models to produce the first gridded climate datasets of key hydroclimatic variables in Ireland, namely reference evapotranspiration, actual evapotranspiration and soil moisture deficits. The Met Éireann Re-Analysis (MÉRA) dataset (Gleeson et al, 2017; Whelan et al, 2018) has been used in this study, alongside the COSMO-CLM5 and WRF v3.7.1, which have been produced by researchers at the Irish Centre for High End Computing (ICHEC), and cover a period of 1981-mid 2018 for MÉRA, and up to 2017 for COSMO-CLM and WRF. MÉRA has a resolution of 2.5 km, whereas COSMO-CLM and WRF have higher resolutions of 1.5 km and 2 km respectively, but lack the data assimilation techniques used in MÉRA.

2 Methodology

Reference evapotranspiration (ET_0) was calculated using the Penman Monteith equation, which is considered to be the international best practice. ET_0 was calculated using variables from all three NWP datasets and interpolated to the 22 synoptic stations across Ireland. ET_0 was calculated from weather observations. As each of the models had biases in the input variables, these had to be corrected. The timeseries for each location was split corresponding to months of the year, from which a least squared estimator could be applied to each month creating a line of best fit. The correction factors therein were then interpolated onto the corresponding model grids, to derive a definitive ET_0 dataset for each model.

Following this, actual evapotranspiration (ET_a) and soil moisture deficits (SMD) were calculated using the Hybrid Soil Moisture Deficit Model (HSMD) which has been implemented at Met Éireann since 2006. Its current commercial version has three drainage classes (well, moderate, poor) and assumes a uniform drainage class across the country, resulting in three maps for SMD each corresponding to a unique drainage class. A newer version, with two additional drainage classes (imperfect, excessive), has been implemented for this study, resulting in five maps of ET_a and SMD corresponding to each drainage class. High resolution (1km spatial resolution) precipitation datasets were used as inputs to the HSMD model. Additionally, the indicative soil drainage map for Ireland has been used to create a sixth map which gives a more realistic estimate of the drainage conditions at each location. All of

these datasets have been produced for daily, monthly, seasonal and annual timesteps, including averages and summed values where applicable.

3 Results

Reference Evapotranspiration (ET_0)

Following the corrections, all models were found to perform with a high degree of accuracy and were in good agreement with ET_0 values calculated from weather observations. Prior to validation, it was expected that MÉRA would outperform both WRF and COSMO-CLM datasets due to the advantage of data assimilation. COSMO-CLM and WRF were however expected to add value due to the higher spatial resolutions (1.5 km and 2 km, respectively) compared to MÉRA (2.5 km). Table 1 shows that MÉRA outperforms both the WRF and COSMO-CLM models for both root mean square error (RMSE) and correlation coefficients across all 22 synoptic stations, each of which has been validated. Figure 1 shows average annual sums of ET_0 across the country for COSMO-CLM, WRF and MÉRA models.

Table 1:Errors in daily and yearly accumulated values of ET_0 for 1981-2017using an overall weighted average across 22 stations.

	RMSE			Standard Deviation			Correlation Coefficient		
Model	COSMO -CLM	WRF	MÉRA	COSMO -CLM	WRF	MÉRA	COSMO -CLM	WRF	MÉRA
Daily	0.442	0.402	0.337	0.882	0.937	0.924	0.892	0.913	0.939
Annual	24.164	21.293	20.402	12.301	14.035	14.813	0.561	0.678	0.755

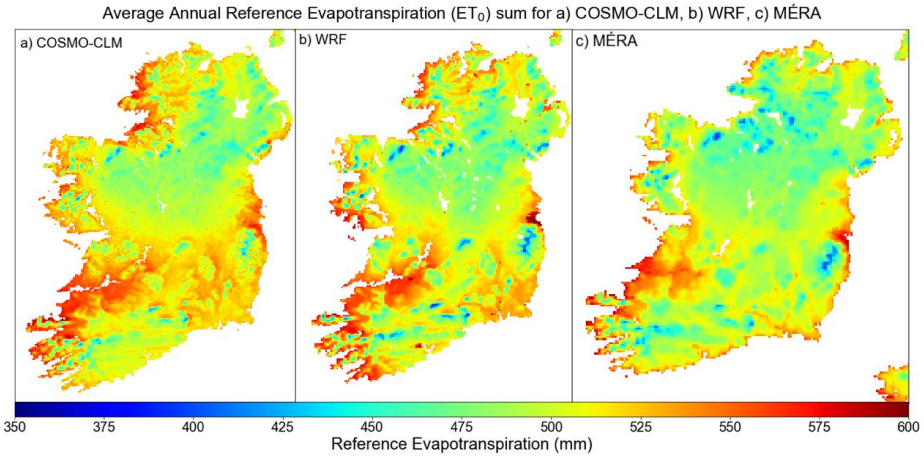

Figure 1: Average Annual ET_0 maps for COSMO-CLM, WRF (1981-2017) and MÉRA (1981-2016).

Actual Evapotranspiration (ET_a)

ET_a has higher applicability to environmental impact assessments, groundwater recharge and other aspects of hydrological modelling. In total, six datasets have been produced for ET_a corresponding to each of the five drainage classes in the HSMD model and the indicative soil drainage map. Table 2 shows errors in ET_a for well drained soils and shows that MÉRA outperforms COSMO-CLM and WRF. As for ET_0, the modelled values for ET_a correspond well with values calculated from the HSMD model. The same analysis was carried out for the moderately drained and poorly drained classes. Figure 2 shows average annual sums of ET_a across the country for COSMO-CLM, WRF and MÉRA using the indicative soil drainage map.

Table 2: Errors in daily and yearly accumulated values of ET_a for well drained soils for 1981-2016 using an overall weighted average across 22 stations

	RMSE			Standard Deviation			Correlation Coefficient		
Model	COSMO -CLM	WRF	MÉRA	COSMO -CLM	WRF	MÉRA	COSMO -CLM	WRF	MÉRA
Daily	0.378	0.347	0.291	0.713	0.740	0.735	0.874	0.896	0.927
Annual	18.024	16.148	15.597	22.759	21.624	20.947	0.745	0.785	0.805

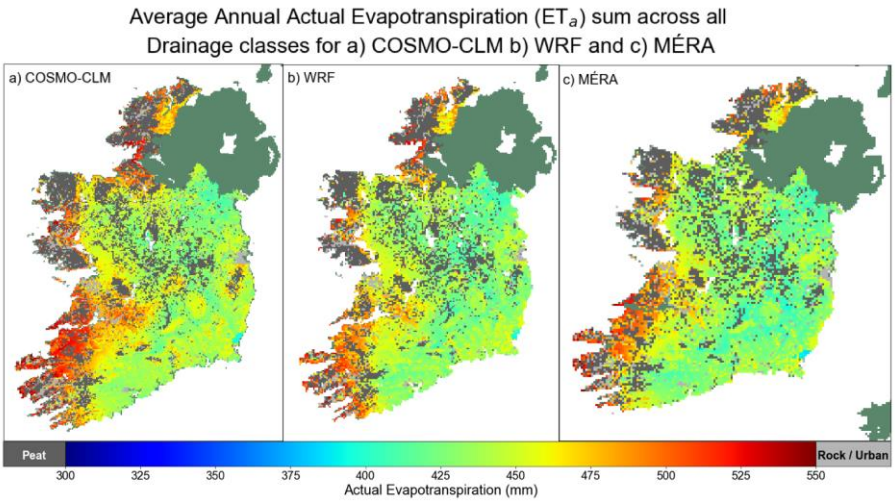

Figure 2: Average Annual indicative ET_a maps for COSMO-CLM, WRF and MÉRA.

Soil Moisture Deficits

As with ET_a, soil moisture deficits (SMD) these have been calculated using the HSMD model for five drainage classes. There is a very good match between SMD calculated using observations and modelled SMD using high-resolution precipitation data. Additionally, the models themselves are in excellent agreement and there is only a small difference in errors. For well drained soils using MÉRA, RMSE values range from 0.339 mm in January to 2.324 mm in June. For most drainage classes, MÉRA still outperforms both WRF and COSMO-CLM both for RMSE and correlation coefficents. The exception is the poorly drained soil class, where values for MÉRA are noticably lower than WRF, COSMO-CLM and the values calculated from weather observations. For this drainage class, WRF is the best performer. Figure 3 shows indicative mean monthly SMD using the indicative soil drainage map.

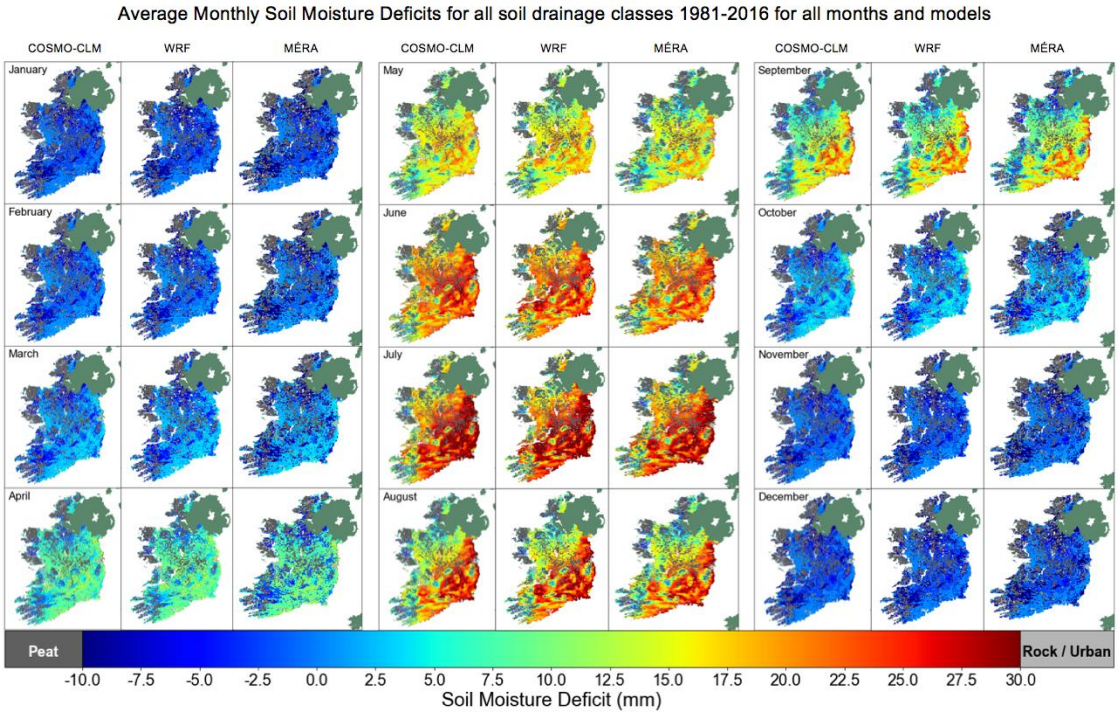

Figure 3: Mean Monthly SMD for all soil drainage classes using WRF, COSMO-CLM and MÉRA (1981- 2016)

4 Summary

High resolution gridded datasets of reference evapotranspiration (ET_0), actual evapotranspiration (ET_a) and soil moisture deficits (SMDs) have been produced using inputs from three NWP models. Reference evapotranspiration (ET_0) was calculated using modelled data as input to the Penman Monteith equation, in line with international best practice, and the current ET_0 calculation method used by Met Éireann and repeated for actual evapotranspiration (ET_a) and soil moisture deficits (SMDs). The results have shown that all models performed well and have been able to capture hydrological variables to a high degree of accuracy. Datasets derived from MÉRA input variables proved to be the most accurate. These datasets will be available online so that they can be utilised by the general public, policy makers and researchers. Any queries can be directed to christopher.werner@ichec.ie.

5 References

Gleeson, E., Whelan, E., and Hanley, J.: Met Éireann high resolution reanalysis for Ireland, Adv. Sci. Res., 14, 49–61, doi:10.5194/asr-14-49-2017, 2017.

Whelan, E., E. Gleeson, and J. Hanley: An evaluation of MÉRA, a high resolution mesoscale regional reanalysis. J. Appl. Meteor. Climatol., In press, https://doi.org/10.1175/JAMC-D-17-0354.1, 2018.

Analysis of historical climate data for Ireland and its impact on Late Blight of potatoes

Joan de Lacey[1], Eoin Lettice[2,3]
[1] BlightLink
[2] School of Biological, Earth and Environmental Sciences (BEES), University College Cork
[3] Environmental Research Institute (ERI), University College Cork

1 Introduction

Late blight of potato is caused by the oomycete *Phytophthora infestans* and is a major pathogen of the Irish and European potato crop. Annual losses in the European Union have been estimated at more than €1 billion (Haverkort *et al*., 2008). The first objective of this research project is to analyse the relative humidity data of the MÉRA reanalysis dataset (Gleeson et al, 2017; Whelan et al, 2018). Relative humidity is of significance in plant health and physiology, occurrence of disease and hence agricultural economic yield. Comparison with historical meteorological data recorded at Irish weather stations will enable any bias in the MÉRA data set to be quantified. Other variables to be considered include temperature, total precipitation and the derived effective blight hours (EBH). The results will provide valuable historical information on potato late blight risk by location in Ireland. This project will build on the work of Bourke (1953) and Keane (1982) who published the average accumulated effective blight hours for the period 1957 to 1981 for Ireland. It will also supplement that of contemporary researchers Cucak *et al*. (2017) and Samala *et al.* (2017).

2 Previous analysis of effective blight hours

The Irish Rules as developed by Bourke (1953) have formed the basis of potato blight forecasting since the 1950s in Ireland and take into account the effect of temperature, relative humidity and the presence of precipitation during a defined period on the epidemiology of the blight causing pathogen *Phytophthora infestans*. Met Éireann currently uses a revised version of Bourke's 'Irish Rules' and synoptic weather maps to predict when blight-favourable conditions are due to arrive. Since the 'Irish Rules' original conception, the pathogen responsible for potato late blight has evolved in to new genotypes, become resistant to certain fungicides and is active at a greater temperature range. Researchers at Teagasc are currently conducting a research study to elucidate changes in the life cycle of the pathogen and to propose a revised blight model for Ireland (Cucak *et al.*, 2017).

The value of an accurate blight model is that it should enable growers to move from a predominantly calendar based spraying schedule, to one where fungicides are used only where necessary in advance of a blight period. This is important from both an economic and environmental standpoint and meets the growing demand from national and EU legislation for growers to more fully adopt an integrated pest/pathogen management (IPM) approach (Lamichhane *et al*., 2016). However, reliance on a blight model has risks. The pathogen is incredibly virulent and once it is established it may result in significant loss of the potato crop. Organic farmers are particularly vulnerable to crop losses as shown in Finland in 2004 where no marketable yield of maincrop organic potatoes were harvested due to a late blight epidemic (Schepers & Spits, 2005).

The link between the activity of the pathogen and humidity has been long established (Bourke, 1993). This was reaffirmed by Iglesias *et al*. (2010) who, in a study comparing different models and spore concentrations, found that the meteorological parameters with the greatest influence on the pathogen are minimum temperature and humidity. Samala (2017) found a reduced potato crop yield in years of high annual rainfall. The proposed study builds on the work regarding accumulation of effective blight hours

(EBH) by Keane (1982) and a preliminary study by de Lacey (2014).

Analysis of Keane (1982)

Keane (1982) through climatic analysis over a period of 25 years (1957 – 1981) found that some areas of Ireland consistently experienced high EBH with a low coefficient of variation. He made the case that in regions such as this regular spraying was advisable, whereas in areas of consistently low EBH spraying according to a warning system could be more economically beneficial. His analysis showed a clear north-south gradient in EBH accumulations with an increase in values near the coast. Minimum values were found in the south midlands and parts of the east of Ireland, where a 10-day cohort analysis across the blight season (May – Sep) showed year-on-year regular blight free periods when spraying to a calendar would be unnecessary. The analysis used 14 synoptic weather stations.

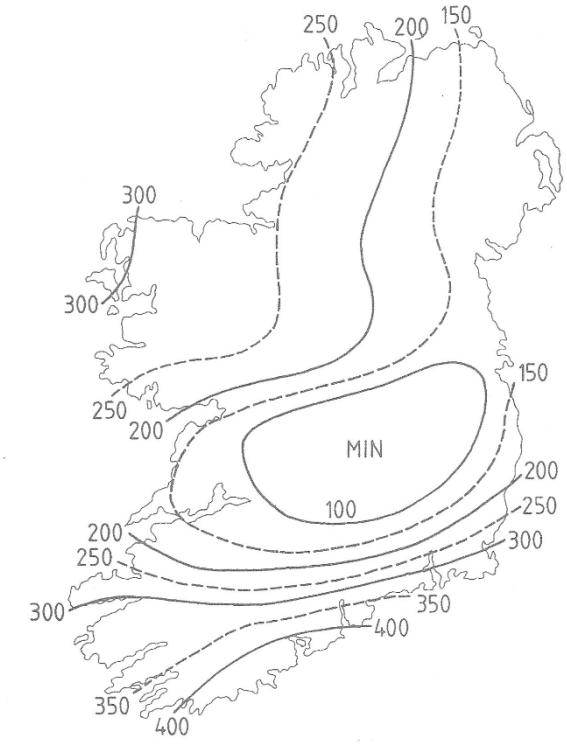

Figure 1: Average (1957-81) accumulations of effective blight hours, May to Sept. (Keane, 1982).

Keane estimated the cost of a routine 14-day spray schedule on Ireland's 40,000 hectares of potatoes between May and September in 1982 at £2.8 million (£10 per hectare per application). Since 1982 the acreage of potatoes has reduced and according to Bord Bia it is now 12,000 ha maintained by 600 growers (https://www.bordbia.ie). De Wolf and van der Klooster (2006) estimate the average cost of late blight control chemicals at 370 €/ha, which would provide an estimate of €4.4 million in costs of control chemicals in Ireland. To put the problem of late blight into perspective, losses in the EU equate to €1 billion; a significant proportion of the farm gate price of €6 billion and consumer price of €15 billion (Haverkort, 2008).

Analysis of de Lacey (2014)

The current planned analysis of the MÉRA dataset builds on a preliminary study of blight risk in west Cork by de Lacey (2014), where meteorological data, provided by Met Éireann for Sherkin Island and Newforge Belfast weather stations, were analysed for EBH over a three year period, 2010 to 2012. During the year with the lowest rainfall (2010), widely reported as a dry year for Ireland, Sherkin Island experienced the highest humidity of the three year period. Comparison with meteorological data for Belfast showed that in extract in 2010 Belfast experienced the lowest humidity of the three years. To confirm the analysis a qualitative comparison was made of blight warning reports issued by Met Éireann

for Sherkin Island and DARD (the Department of Agriculture and Rural Development) for Belfast, where modified Smith infection periods are reported. The occurrence of the high levels of humidity at Sherkin Island would suggest that Sherkin Island and the surrounding area in west Cork were at a greater risk to infection by *P. infestans* even during 2010, a relatively dry year.

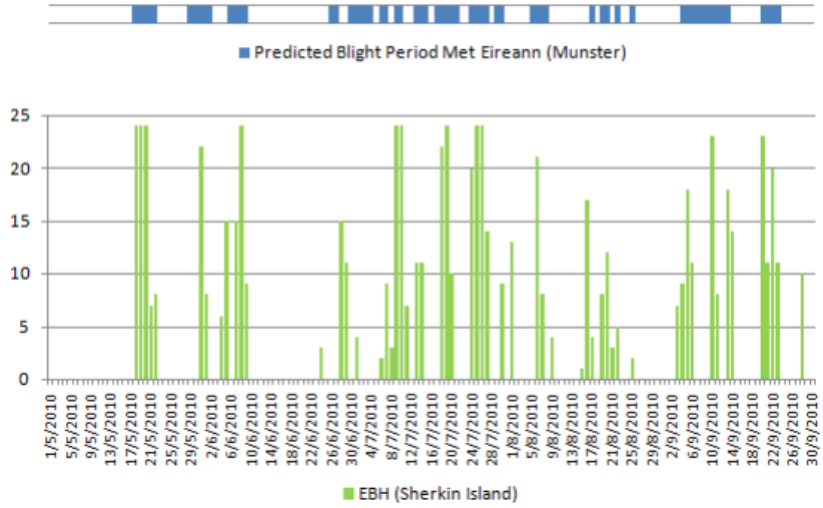

Figure 2: EBH for Sherkin Island vs. Met Éireann blight warning reports for 2010 (de Lacey, 2014).

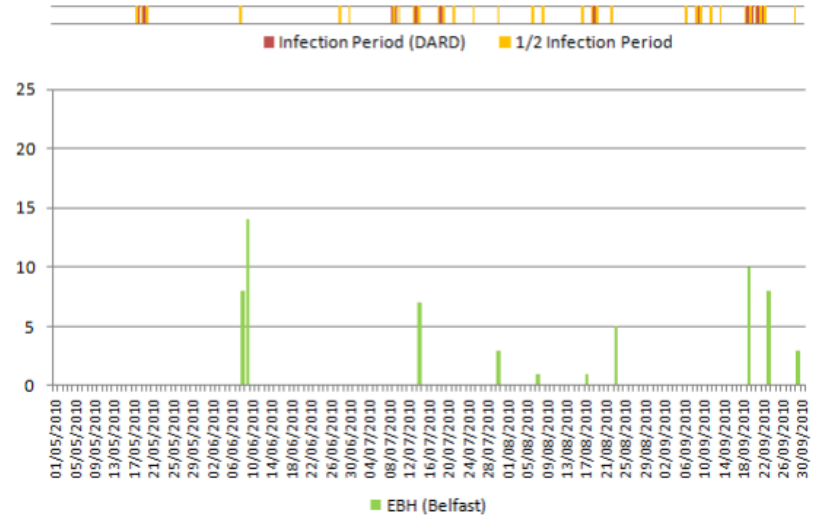

Figure 3: EBH for Belfast vs DARD infection periods for 2010 (de Lacey, 2014).

The high value of EBHs for Sherkin Island is consistent with the observations of Keane who found this area of Ireland to experience average annual accumulations of EBH in excess of 400 hours, with the area around Belfast experiencing the lowest in Ireland at less than 150 hours. De Lacey (2014) conjectured that the high EBH observed on Sherkin Island, associated with a relatively dry year, was due to sea fog. Sea fog brings moist, cool, humid conditions, suitable for the germination of the *P. infestans* sporangia, and may also act as transport for sporangia and potentially the spread of late blight.

Figure 4: Sea fog intrusion, mainland adjacent to Sherkin Island, West Cork.

3 Planned analysis and applications

Our study aims to repeat the analysis of Keane (1982) using the MÉRA reanalysis data to extend Keane's previous 25 year analysis of EBH (1957 – 1981), a further 35 years to 2016. Will we observe the same spatial distribution of EBH? What is the relationship between the individual variables of temperature, relative humidity, precipitation and EBH for different regions of Ireland? The results of our analysis of the MÉRA reanalysis dataset for blight risk will have implications not only for commercial growers but also help to inform backyard growers.

Zwankhuizen (1998) identified allotments as a minor source of blight for farmers. In 2009 a pandemic in the United States was caused by a single wholesale nursery distributing infected tomato transplants across the Northeast and mid-Atlantic regions of the United States (Fry *et al*., 2012). The synchronous release resulted in 13 states being infected with late blight. The driver was mainly a lack of knowledge regarding potato late blight, on the part of the plant nurseries and backyard growers. As a result of the analysis of the MÉRA data, information will be available to backyard growers regarding the historic risk of blight for their location. Backyard growers in areas of significant risk, who are growing organically, can be encouraged to adopt resistant cultivars to prevent the spread of blight to neighbouring farms. Scenario analysis by Pically *et al*. (2016) found that engagement of all stakeholders and a change in market demand to resistant potatoes, would result in a reduction in the severity of blight outbreaks.

A further application is that the knowledge gained from the analysis will help to inform the release of BlightLink (http://blightlink.com/) a mobile application, which provides hourly, location specific, forecast information regarding blight risk for growers. In areas where the variability of EBH is found to be consistently high, growers will be advised that the App will act only as a fore-warning of ensuing blight periods. In areas with low variability and low blight risk, BlightLink may act to reduce unnecessary sprays of fungicide, particularly when combined with the function of enabling users to report blight outbreaks, therefore providing additional information on blight pressure in an area. This is particularly important in the light of future erratic weather pattern predictions (Samala, 2017).

Observations of pests and pathogens have shown a movement towards the poles at a rate of 2.7 ± 0.8 km yr^{-1} since the 1960s (Bebber *et al*., 2013). Potato late blight has been highlighted as a potential threat to global food security, particularly when one considers the recent observations in Europe of more virulent genotypes, the global reliance on the potato crop (3rd largest crop), and the increase in acreage worldwide (https://www.teagasc.ie/crops/crops/potatoes). The analysis of the MÉRA reanalysis dataset may reveal the impact of climate change on the risk of late potato blight for Ireland, provide a benchmark for ongoing monitoring, and inform future adaptations to climate change.

Websites:
BlightLink – https://blightlink.com
Bord Bia website - https://www.bordbia.ie/consumer/aboutfood/veg/potatoes/pages/default.aspx/
Teagasc - https://www.teagasc.ie/crops/crops/potatoes/potato-blight-disease/

4 References

Bebber, D. P., Ramotowski, M. A. T. & Gurr, S. J. (2013). Crop pests and pathogens move polewards in a warming world. *Nature Climate Change*. DOI:10.1038/NCLIMATE19 90.

Bourke, A (1953). Potato blight and the weather: a fresh approach. Irish Meteorological Service.

Bourke, A and Lamb, H (1993). The spread of potato blight in Europe 1845-6 and the accompanying wind and weather patterns. Irish Meteorological Service.

Cucak, M., Sparks, A. H., Fealy, R., Griffin, D., Lambkin, K. and Kildea, S. (2017). The use of agrometeorological data for crop disease risk forecasting in Ireland: a case of potato late blight. Dept. of Geography, National University of Ireland Maynooth. Teagasc. (EMS2017-428).

de Lacey, J. (2014). A decision support system for the control of *Phytophthora infestans* in West Cork. MSc Thesis, School of Biological, Earth and Environmental Sciences, University College Cork.

De Wolf M, and van de Klooster A (2006). Kwanitatieve Informatie Akkerbouw en Vollegrondsgroenteteelt. KWIN AGV, (http://www.ppo.wur.nl/NL/publicaties/), PPO 354.

Fry, W. E., McGrath, M. T., Seaman, A., Zitter, T. A., McLeod, A., Danies, G., Small, I., Myers, K., Everts, K., Gevens, A., Gugino, B. K., Johnson, S., Judelson, H., Ristaino, J., Roberts, P., Secor, G., Seebold, K., Snover-Clift, K., Wyenandt, A., Grunwald, N. J. and Smart, C. D. (2012). The 2009 Late blight pandemic in Eastern USA. APS Features. doi:10,1094/APSFeature-2012-08.

Gleeson, E., Whelan, E., and Hanley, J.: Met Éireann high resolution reanalysis for Ireland, Adv. Sci. Res., 14, 49–61, doi:10.5194/asr-14-49-2017, 2017.

Haverkort, A. J., Boonekamp, P. M., Hutten, R., Jacabsen, E., Lotz, L. A. P., Kessel, G. J. T., Visser, R. G. F. and van der Vossen, E. A. G. (2008). Societal costs of late blight in potato and prospects of durable resistance through cisgenic modification. *Potato Research* 51:47-57.

Iglesias, I, Escuredo, O and Seijo, C. (2009). *Phytophthora infestans* prediction for a Potato Crop. *Am. J. Pot. Res*. **87**, 32 – 40.

Keane, T (1982). Weather and potato blight. *Irish Meteorological Service.*

Lamichhane, J.R., Dachbrodt-Saaydeh, S., Kudsk, P., Messean, A. (2016). Toward a reduced reliance on conventional pesticides in European agriculture. *Plant Disease* 100: 10-24.

Pically, F. C. A., Groot, J. C, Hofstede, G. J., Schaap, B. F. and Lammerts van Bueren, E. T. (2016). Analysing potato late blight control as a social-ecological system using fuzzy cognitive mapping. *Agron. Sustain. Dev*. 36: 35.

Samala, B. K., McKinstry, A. and Nolan, P. (2017). The impact of Climate on potato crop in Ireland: A case study. Irish Centre for High End Computing. (EMS2017-667).

Schepers, H. T. A. M. and Spits, H. G. (2005). The development and control of *Phytophthora infestans* in Europe in 2004- 2005. Ninth Workshop of a European Network for development of an Integrated Control Strategy of potato late blight, Tallinn, Estonia. *PPO-Special Report no. 11*:11-12.

Whelan, E., E. Gleeson, and J. Hanley: An evaluation of MÉRA, a high resolution mesoscale regional reanalysis. J. Appl. Meteor. Climatol., In press, https://doi.org/10.1175/JAMC-D-17-0354.1, 2018.

Zwankhuizen, M. J., Govers, F. and Jan C. Zadoks (1998). Development of Potato Late Blight Epidemics: Disease Foci, Disease Gradients, and Infection Sources. *Phytopathology*. 754-763.

High spatio-temporal resolution dry deposition velocity mapping using the MÉRA dataset

Kayla Wilkins[1], Hazel Cathcart[1], Julian Aherne[1]
[1] Trent University

1 Introduction

There is a growing concern that atmospheric emissions of gaseous nitrogen (N) compounds, such as ammonia, from the agricultural industry, are negatively impacting plant biodiversity in natural ecosystems in Ireland (Henry & Aherne, 2014; Stevens et al., 2011; Wilkins & Aherne, 2016; Wilkins et al., 2016). Atmospheric emissions ultimately return to the Earth's surface via deposition, either in rainfall (wet deposition) or by dry fallout (dry deposition). Globally, elevated N deposition has been demonstrated to have a negative impact on plant species diversity (Bobbink et al., 2010; Roth, et al., 2015; Wallis de Vries et al., 2017), suggesting that N deposition may directly impact national commitments under the Habitats Directive (European Commission, 2015). The National Emission Ceilings Directive (NEC Directive) has recently required all member states to establish a network of ecosystem sites to evaluate the impact of air pollutants on natural or semi-natural ecosystems (EEA, 2016a); national ammonia emissions are perhaps of most concern in this respect.

Effectively evaluating the impact of air pollutants, including ammonia, on natural ecosystems requires accurate estimates of wet and dry atmospheric deposition. In Ireland, wet N deposition is widely monitored; Met Éireann has actively monitored precipitation since the late 1950s at a number of monitoring stations (Tierney, 1967; Mathews & McCaffrey, 1977). There are currently five stations monitoring wet deposition (Belmullet, Johnstown Castle, Malin Head, Oak Park, and Valentia Observatory). However, dry N deposition is not easily measured, and is generally estimated from the product of air concentration and deposition velocity (i.e. the rate at which gases or particles are transferred to a given surface, V_d). Air concentrations of certain pollutants (including ammonia) have been measured in Ireland (e.g., de Kluizenaar & Farrell, 2000), whereas estimates of V_d have been taken from generalised landscape-based literature values (Henry & Aherne, 2014; Wilkins & Aherne, 2016; Wilkins et al., 2016), which vary considerably for ammonia (Schrader & Brümmer, 2014). High resolution maps of V_d would greatly improve estimates of dry and total deposition, in particular for nitrogen species.

The processes that contribute to the V_d of a gas or particle onto a given surface, particularly a heterogeneous surface, are complex, and influenced by the characteristics of the particle type, the qualities (e.g., roughness) of the receptor surface, and the micro-climate at the site of deposition (Hicks et al., 2016; Petroff et al., 2008; Pryor et al., 2008; Wesely & Hicks, 2000). Deposition velocity can be inferred from eddy correlation measurements; however, this method has a number of challenges (Businger, 1986; Finkelstein & Sims, 2001; Pryor et al., 2008). There is a reliance on computer modelling to estimate V_d. The 'Big Leaf' model developed by Zhang and others (Petroff & Zhang, 2010; Zhang & He, 2014; Zhang et al., 2001; Zhang et al., 2003) has been shown to perform well compared to V_d measurements (Szinyei et al., 2018; Zhang et al., 2001; Zhang et al., 2002), and has been widely applied (Adon et al., 2013; de Vos & Zhang, 2012; Flechard et al., 2011; Yu et al., 2013). This model does, however, require a number of meteorological input variables (Table 1), previously unavailable at high-spatial resolution on a national scale. The publication of Met Éireann's climate re-analysis dataset, MÉRA, (Gleeson et al., 2017; Whelan et al, 2018) has made mapping of V_d on a national scale possible.

Here we demonstrate how the recently published MÉRA climatological dataset can be used to estimate V_d for 31 gaseous species, including ammonia, and three particulate size classes, leading to high spatial resolution national maps. In combination with observations of the atmospheric concentration of gases and particles, these velocities can be used to generate national dry deposition maps for atmospheric pollutants.

2 Methods

The V_d model requires hourly inputs for nine climatic variables (Table 1), the landcover (for 26 landcover types) and location (latitude) where the climatic variables were observed or estimated. Climatic input data for the model were predominantly sourced from Met Éireann's climate reanalysis project (Gleeson et al., 2017). Climate reanalysis data are available from 1981 to mid-2018 at a 2.5 km resolution for Ireland produced using the ALADIN-HIRLAM numerical weather prediction system (www.hirlam.org). In the current study, the V_d model was run at three-hour intervals for each 2.5 km grid point across Ireland for the period June 2013 to July 2014, which coincided with the operation of a national ammonia monitoring network (Doyle et al., 2017). The Big Leaf model requires proportional area data for 26 landcover classes, which were calculated for each 2.5 km grid using landcover data extracted from the CORINE 2012 map (1:250 000) (EEA, 2016b). Snowfall was assumed to be zero; cloud fraction was set to 1 (100% cover) as the MÉRA data were unavailable at the time of the study. However, model results were not sensitive to cloud cover under the climate conditions typical to Ireland.

Table 1: Inputs required by the 'Big Leaf' dry deposition velocity model and their data sources

PARAMETER	**SOURCE**
Temperature at 2 m	MÉRA
Surface temperature	MÉRA
Precipitation rate	MÉRA
Windspeed at 10 m	MÉRA
Surface pressure	MÉRA
Humidity	MÉRA
Solar irradiance	MÉRA
Cloud fraction	Set to 1
Snow depth	Assumed to be zero
Landcover	CORINE 2012

3 Results and discussion

Annual averaged dry deposition velocity maps were created from the model output (average of 3,408 3−hourly estimates) on a 2.5 km × 2.5 km grid, which represents the highest spatio-temporal resolution V_d maps for Ireland to date. In general, annual average V_d for ammonia (NH_3), sulphur dioxide (SO_2), ozone (O_3) and nitrogen dioxide (NO_2) show higher values in upland areas along the west coast, particularly Donegal, Mayo, Galway and Kerry and in eastern regions such as the Wicklow Mountains (Figure 1). The influence of climatic factors is clear in these annual maps, as regions with higher V_d coincide with regions of greater windspeed, which appeared to be a particularly influential driver of V_d. Elevated V_d is also clearly seen during events with elevated wind speeds in the east-west and north-south vectors in the time-series dataset; for example, 03:00 hours on June 6, 2013 illustrated an elevated V_d response to east-west gusts beginning to make their way eastward across the country (Figure 2). Annual average V_d values during 2013–2014 for Ammonia (NH_3) and Sulfur Dioxide (SO_2) were 0.808 and 0.758 cm s^{-1} respectively; Ozone (O_3) and Nitrogen Dioxide (NO_2) represent lower V_d at 0.399 and 0.348 cm s^{-1} respectively (Table 2).

It is important to note that the national average annual V_d values do not represent site-specific V_d because average values summarise all landcover classes across the country and are influenced by the proportion of grasslands in Ireland. It is also crucial to recognise that areas of high dry V_d do not necessarily correspond to areas of high dry deposition; it is possible to have regions that experience high dry V_d but low pollutant air concentrations, resulting in low dry deposition.

Table 2: Summary statistics for annual ammonia (NH_3), sulphur dioxide (SO_2), ozone (O_3), and nitrogen dioxide (NO_2) dry deposition velocity (cm s^{-1}) for Ireland during the period June 2013 to July 2014

	NH_3	**NO_2**	**O_3**	**SO_2**
Mean	0.808	0.348	0.399	0.758
Median	0.737	0.354	0.403	0.691
Minimum	0.073	0.023	0.028	0.069
Maximum	1.698	0.711	0.837	1.608
Standard deviation	0.186	0.084	0.098	0.177

The 3-hourly modelled V_d shows high temporal variability. For example during the first week of July 2013 in Glendalough National Park, Wicklow (located in an area of high annual average V_d, see Figure 1), V_d ranged from less than 0.5 cm s^{-1} to nearly 2.5 cm s^{-1} (Figure 3). The lowest V_d values were observed on July 3, and coincided with a calm period with low east–west and north–south windspeeds in the MÉRA dataset. In addition, landscape-based V_d values exhibit a similar range for different habitat types (e.g. 0.5 cm s^{-1} for grasslands versus 2.5 cm s^{-1} for deciduous woodlands), highlighting the importance of site-specific and time-specific V_d estimates.

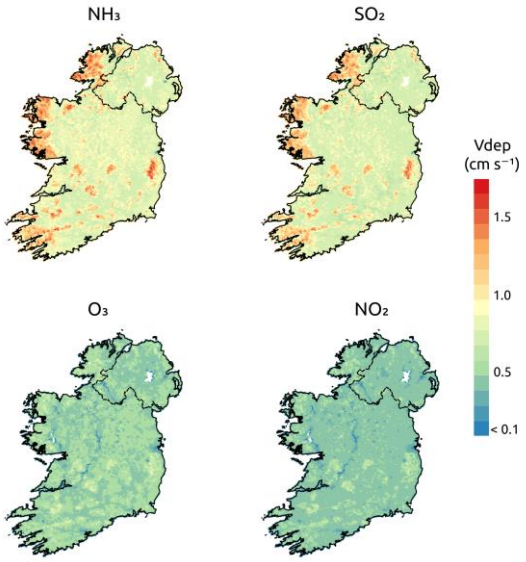

Figure 1: Annual average dry deposition velocity (cm s–1) of ammonia (NH3), sulphur dioxide (SO2), ozone (O3), and nitrogen dioxide (NO2) for Ireland.

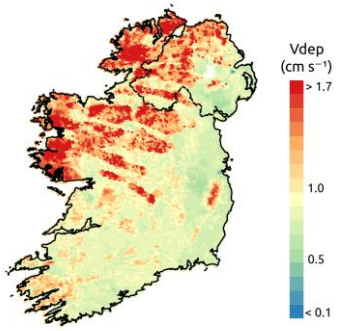

Figure 2: Elevated dry deposition velocity (V_d) response to westerly winds on June 2, 2013 at 03 00 UTC.

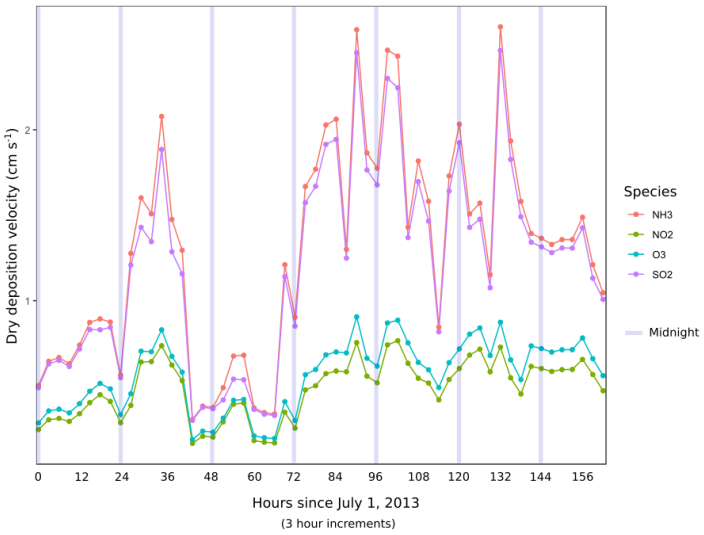

Figure 3: Modelled dry deposition velocity (cm s^{-1}) for ammonia (NH_3), sulphur dioxide (SO_2), ozone (O_3), and nitrogen dioxide (NO_2) at Glendalough National Park in Wicklow, Ireland during the first week of July 2013.

4 Conclusions

MÉRA data were used to model dry deposition velocities for 31 gaseous species and 3 particulate matter size classes on a 2.5 km grid across Ireland at 3,408 3-hourly intervals for one annual cycle. The resulting series of dry deposition velocity maps demonstrated the influence of meteorology and land cover on the seasonal deposition velocities for gaseous and particulate species.

High-resolution V_d estimates are only one part of the requirements for estimating dry deposition, which is the product of V_d and air concentrations. There is a growing need for accurate estimates of total N deposition as cattle density increases in response to the Department of Agriculture, Food, and the Marine's Food Harvest 2020 (DAFM, 2010), concurrent with commitments under the NEC Directives for Member States to evaluate and report on the impact of air pollutants to semi-natural ecosystems, and the reporting of habitat status under the Habitats Directive.

5 References

Adon, M., Galy-Lacaux, C., Delon, C., Yoboue, V., Solmon, F., & Kaptue Tchuente, A. T. (2013). Dry deposition of nitrogen compounds (NO2, HNO3, NH3), sulfur dioxide and ozone in west and central African ecosystems using the inferential method. Atmospheric Chemistry and Physics, 13(22), 11351–11374. https://doi.org/10.5194/acp-13-11351-2013

Bobbink, R., Hicks, K., Galloway, J., Spranger, T., Alkemade, R., Ashmore, M., … de Vries, W. (2010). Global assessment of nitrogen deposition effects on terrestrial plant diversity: a synthesis. Ecological Applications, 20(1), 30–59.

Businger, J. A. (1986). Evaluation of the accuracy with which dry deposition can be measured with current micrometeorological techniques. Journal of Climate and Applied Meteorology, 25(8), 1100–1124.

DAFM – Department of Agriculture, Food, and the Marine. (2010). Food harvest 2020: A vision for Irish agri-food and fisheries.
URL: http://www.agriculture.gov.ie/foodwise2025/foodharvest2020/. Accessed 27.02.2017.

de Kluizenaar, Y., Farrell, E.P. (2000). Ammonia Monitoring in Ireland. Environmental Protection Agency, Wexford, Ireland.

de Vos, T., & Zhang, L. (2012). High resolution mapping of total deposition of acidifying pollutants. Atmospheric Environment, 57(Supplement C), 80–90. https://doi.org/10.101

Doyle, B., Cummins, T., Augustenborg, C., & Aherne, J. (2017). Ambient Atmospheric Ammonia in Ireland, 2013-2014 (EPA Research Report No. 193). Wexford, Ireland: Environmental Protection Agency. Retrieved from
http://www.epa.ie/pubs/reports/research/air/EPA%20RR%20193%20Essentra%20web%20(1).pdf

European Commission. (2015). The Habitats Directive: about the Habitats Directive. URL:
http://ec.europa.eu/environment/nature/legislation/habitatsdirective/. Accessed 01.07.18.

EEA − European Environment Agency, European Union. (2016a). National Emission Ceilings Directive. URL: https://www.eea.europa.eu/themes/air/national-emission-ceilings. Accessed 01.07.18.

EEA – European Environment Agency, European Union. (2016b). Corine Land Cover 1:250,000 vector data. URL: https://land.copernicus.eu/pan-european/corine-land-cover/clc-2012. Accessed 22.03.17.

Finkelstein, P. L., & Sims, P. F. (2001). Sampling error in eddy correlation flux measurements. Journal of Geophysical Research: Atmospheres, 106(D4), 3503–3509. https://doi.org/10.1029/2000JD900731

Flechard, C. R., Nemitz, E., Smith, R. I., Fowler, D., Vermeulen, A. T., Bleeker, A., … Sutton, M. A. (2011). Dry deposition of reactive nitrogen to European ecosystems: a comparison of inferential models across the NitroEurope network. Atmospheric Chemistry and Physics, 11(6), 2703–2728. https://doi.org/10.5194/acp-11-2703-2011

Gleeson, E., Whelan, E., & Hanley, J. (2017). Met Éireann high resolution reanalysis for Ireland. Advances in Science and Research, 14, 49–61. https://doi.org/10.5194/asr-14-49-2017

Henry, J., & Aherne, J. (2014). Nitrogen deposition and exceedance of critical loads for nutrient nitrogen in Irish grasslands. Science of The Total Environment, 470–471, 216–223. https://doi.org/10.1016/j.scitotenv.2013.09.047

Hicks, B. B., Saylor, R. D., & Baker, B. D. (2016). Dry deposition of particles to canopies—A look back and the road forward. Journal of Geophysical Research: Atmospheres, 121(24), 2015JD024742. https://doi.org/10.1002/2015JD024742

Mathews, R.O. and Mccaffrey, F. (1997). Chemical Analysis of Precipitation in Ireland 1966-1975.

Petroff, A., & Zhang, L. (2010). Development and validation of a size-resolved particle dry deposition scheme for application in aerosol transport models. Geoscientific Model Development, 3(2), 753–769. https://doi.org/10.5194/gmd-3-753-2010

Petroff, A., Mailliat, A., Amielh, M., & Anselmet, F. (2008). Aerosol dry deposition on vegetative canopies. Part I: Review of present knowledge. Atmospheric Environment, 42(16), 3625–3653. https://doi.org/10.1016/j.atmosenv.2007.09.043

Pryor, S. C., Gallagher, M., Sievering, H., Larsen, S. E., Barthelmie, R. J., Birsan, F., … Vesala, T. (2008). A review of measurement and modelling results of particle atmosphere–surface exchange. Tellus B, 60(1), 42–75. https://doi.org/10.1111/j.1600-0889.2007.00298.x

Roth, T., Kohli, L., Rihm, B., Amrhein, V., & Achermann, B. (2015). Nitrogen deposition and multi-dimensional plant diversity at the landscape scale. Royal Society Open Science, 2(4), 150017. https://doi.org/10.1098/rsos.150017

Schrader, F., & Brümmer, C. (2014). Land Use Specific Ammonia Deposition Velocities: a Review of Recent Studies (2004–2013). Water, Air, & Soil Pollution, 225(10), 1–12. https://doi.org/10.1007/s11270-014-2114-7

Stevens, C., Duprè, C., Gaudnik, C., Dorland, E., Dise, N., Gowing, D., … Diekmann, M. (2011). Changes in species composition of European acid grasslands observed along a gradient of nitrogen deposition. Journal of Vegetation Science, 22(2), 207–215. https://doi.org/10.1111/j.1654-1103.2010.01254.x

Szinyei, D., Gelybó, G., Guenther, A. B., Turnipseed, A. A., Tóth, E., & Builtjes, P. J. H. (2018). Evaluation of ozone deposition models over a subalpine forest in Niwot Ridge, Colorado. Időjárás, 122(2), 119–143. https://doi.org/10.28974/idojaras.2018.2.2

Tierney, S.L. (1967). Atmospheric Chemistry in The Irish Meteorological Service and a Discussion of Some Results. Technical Note No. 32, Meteorological Service, Department of Transport and Power, Dublin, September 1967.

Wallis de Vries, M. F., & Bobbink, R. (2017). Nitrogen deposition impacts on biodiversity in terrestrial ecosystems: Mechanisms and perspectives for restoration. Biological Conservation, 212, 387–389. https://doi.org/10.1016/j.biocon.2017.01.017

Wesely, M. L., & Hicks, B. B. (2000). A review of the current status of knowledge on dry deposition. Atmospheric Environment, 34(12–14), 2261–2282. https://doi.org/10.1016/S1352-2310(99)00467-7

Whelan, E., E. Gleeson, and J. Hanley: An evaluation of MÉRA, a high resolution mesoscale regional reanalysis. J. Appl. Meteor. Climatol., In press, https://doi.org/10.1175/JAMC-D-17-0354.1, 2018.

Wilkins, K., & Aherne, J. (2016). Vegetation community change in Atlantic oak woodlands along a nitrogen deposition gradient. Environmental Pollution, 216, 115–124. https://doi.org/10.1016/j.envpol.2016.05.024

Wilkins, K., Aherne, J., & Bleasdale, A. (2016). Vegetation community change points suggest that critical loads of nutrient nitrogen may be too high. Atmospheric Environment, 146, 324–331. https://doi.org/10.1016/j.atmosenv.2016.07.016

Yu, X., Driscoll, C. T., Huang, J., Holsen, T. M., & Blackwell, B. D. (2013). Modeling and Mapping of Atmospheric Mercury Deposition in Adirondack Park, New York. PLoS ONE, 8(3), e59322. https://doi.org/10.1371/journal.pone.0059322
6/j.atmosenv.2012.04.037

Zhang, L., Brook, J. R., & Vet, R. (2003). A revised parameterization for gaseous dry deposition in air-quality models. Atmospheric Chemistry and Physics, 3(6), 2067–2082.

Zhang, L., & He, Z. (2014). Technical Note: An empirical algorithm estimating dry deposition velocity of fine, coarse and giant particles. Atmospheric Chemistry and Physics, 14(7), 3729–3737. https://doi.org/10.5194/acp-14-3729-2014

Zhang, L., Gong, S., Padro, J., & Barrie, L. (2001). A size-segregated particle dry deposition scheme for an atmospheric aerosol module. Atmospheric Environment, 35(3), 549–560. https://doi.org/10.1016/S1352-2310(00)00326-5

Zhang, L., Moran, M. D., Makar, P. A., Brook, J. R., & Gong, S. (2002). Modelling gaseous dry deposition in AURAMS: a unified regional air-quality modelling system. Atmospheric Environment, 36(3), 537–560. https://doi.org/10.1016/S1352-2310(01)00447-2

Technical Note No. 42, Meteorological Service, Dublin August 1977

Validation of MÉRA total precipitation at Stornoway (Scotland) with a 24 GHz Micro Rain Radar: A Preliminary Investigation

Edward Graham[1], Chris Kidd[1], and Graham Florence[1]

[1]University of the Highlands and Islands

1 Introduction

A 24 GHz METEK Micro Rain Radar (MRR) has been in operation at the University of the Highlands and Islands, Lews Castle, Stornoway (Hebrides, Scotland) since 2015 (see Figure 1). Located at $58°$N in one of the most frequently rained-upon regions of Britain (with an annual average of ~280 raindays per year), Stornoway lies fully exposed to all weather systems approaching from the North Atlantic Ocean. Similar to western Ireland, there is a very high correlation between the North Atlantic Oscillation (NAO) Index and monthly precipitation anomalies.

This part of north-western Scotland has already seen increases in the order 40% in winter precipitation over the past 40 years (Barnett et al., 2006, Graham 2012). Such gains in precipitation were not expected until the latter half of the 21^{st} century according to climate change model scenarios for the region (Jenkins et al., 2008), and are significantly greater than the expected response of the Clausius-Clapeyron saturation vapour pressure relationship to a modest surface temperature warming of $0.5°$C over the same 40 year period. Therefore, careful and accurate monitoring of precipitation in this sensitive climatic region is paramount for detection and attribution of the manifestations of climate change.

This short paper presents the results of a preliminary investigation into how a combination of the Stornoway Lews Castle MRR and nearby ground-based rain gauges may be used to validate the high resolution MÉRA total precipitation dataset (Glesson et al., 2017; Whelan et al., 2018) for the Stornoway and NW Scotland region. At least four rain gauges are available in close proximity for the ground truthing of the MRR, conventional Met Office radar and reanalysis data. The MRR measures echo reflectivity (dBZ), fall velocity (m/s) and Doppler velocity (m/s) with a derived precipitation rate (mm/h) based on estimated droplet size spectra distributions.

2 The Stornoway Micro Rain Radar (MRR)

The principal motivation behind the installation and operation of the Stornoway MRR is the NASA Global Precipitation Mission (Hou et al., 2014), Stornoway being a key mid-latitude site in the calibration of space-based estimates of rainfall detection and intensity. The Stornoway MRR operates continuously in Frequency Modulation (FM) mode at 24 GHz, with a saw tooth signal sending a vertical pulse of radiation, which is back-scattered (reflected) by hydrometeors (snow, hail, sleet, rain) and possibly aerosols. The vertical resolution of reflection can be adjusted to between 30-100 m, with a maximum vertical height penetration of 3.1 km. Data are averaged over time bins of one minute, meaning the MRR has a spatial and temporal resolution of up to one magnitude greater than traditional meteorological radars. As the wavelength of the radiation (~1.3 cm) is greater than the droplet size, than amount of back scatter is proportional to the 6^{th} power of the droplet radius. Furthermore, since freezing heights above Stornoway often lie close to the surface, and are rarely above

Figure 1: The 24 GHz METEK Micro Rain Radar (MRR) installed at the University of the Highlands and Islands, Stornoway, Scotland.

Table 1: MÉRA, MRR and local rain gauges accumulated precipitation totals for 30 June 2015

Observation	Total (mm)
MÉRA Stornoway (single point only):	6.9
MÉRA whole island (max)	20.5
Micro Rain Radar (MRR)	20.0
Rain gauge No. 1	18.4
Rain gauge No. 2	18.6
Rain gauge No. 1	19.0

3000m, the bright band (~freezing altitude) is easily detected from the resulting Fall Velocity and Doppler shift measurements.

3 Case Study: MRR, MÉRA and UK Met Office radar for 30 June 2015

The Stornoway MRR was installed on 15 June 2015, and a comparison between its data, that of MÉRA, the UK Met Office's Plan Position Radar (PPI) product (Met Office, 2003) and three local rain gauges was attempted for the date of 30 June 2015, as a preliminary study. There was no shortage of rain during summer 2015 in Stornoway (as it was one of the wettest and dullest summers of the past two centuries!). The results of this initial comparison are listed in Table 1, as well as shown in accommpanying Figures 2 and 3.

From Table 1, it can be seen that the MRR total accumulated precipitation for 30 June 2015 was 20.0 mm. The equivalent local rain gauge values were 19.0 mm, 18.6 mm and 18.4 mm, respectively. These slightly lower rain gauge totals are easily accounted for by wind loss or splashing, which is expected to be common at the exposed location of Stornoway. The equivalent Met Office PPI radar total for grid pixels surrounding Stornoway are in the range 15-20 mm.

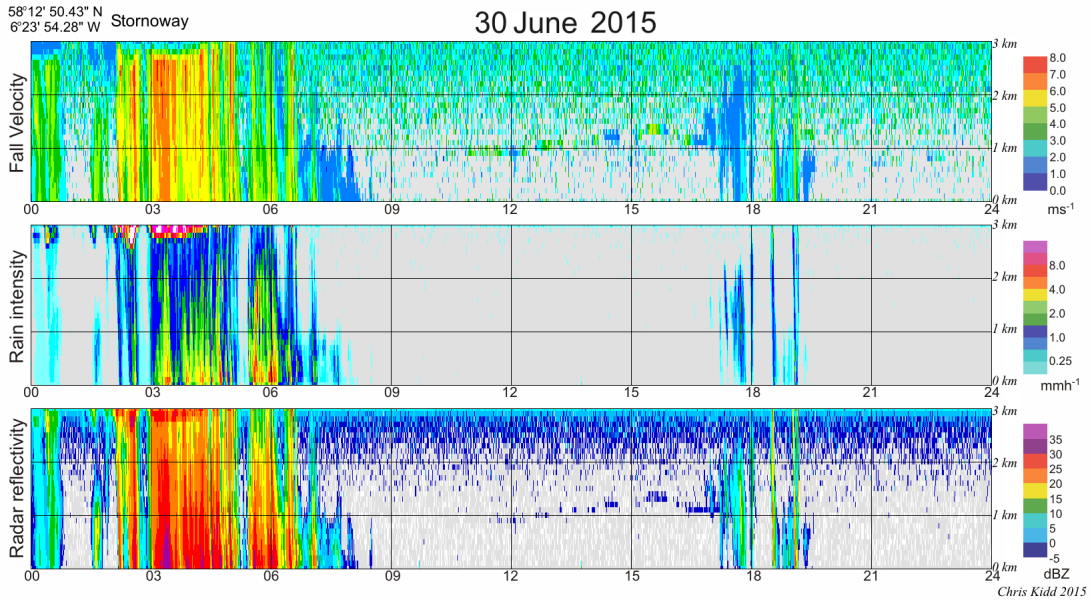

Figure 2: Height versus time plots of the Stornoway MRR on 30 June 2015 for as follows; Top panel: Fall Velocity (m/s); Middle Panel: Precipitation Intensity (mm/h; Bottom panel: Raw radar relfectivity (dBZ).

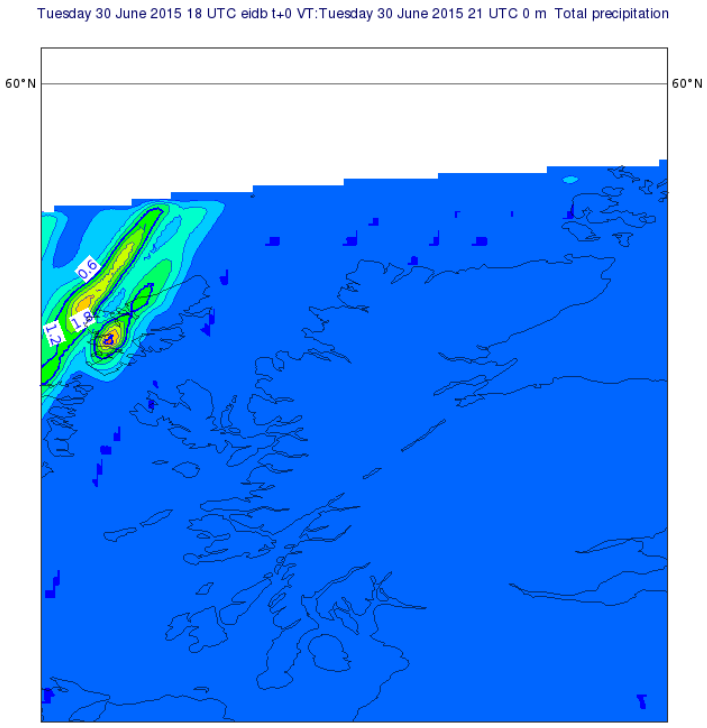

Figure 3: MÉRA total 3-hourly accumlated precipitation from 1800 UTC to 2100 UTC on 30 June 2015.

4 Summary and Conclusions

It is clear that significant precipitation changes are currently afoot in northwestern Scotland. The Stornoway MRR, in combination with MÉRA offer new research opportunities towards the study and analysis of these changes. Whilst the agreement found for the case study of 30 June 2015 is very promising, it is clear in this case that a longer time series of data are needed for a comprehensive climatological analysis and for validation of MÉRA with the MRR and other ground observations. Precipitation is largely a stochastic mesoscale phenomenon, and it would therefore be interesting to see if direct assimilation of this very high resolution radar data product into meteorological models might be possible and advantageous, or if it may continue to pose complications, such as previously with GPS/GNSS high resolution precipitable water vapour fields (e.g. Guerova et al., 2003).

5 Acknowledgments

The authors would like to thank Emily Gleeson (Met Éireann) and Eoin Whelan (Met Éireann), NASA, and the University of the Highlands and Islands (Scotland) Research and Conference Travel Fund. Some of the ground rain gauge data was provided by the Scottish Environmental Protection Agency (SEPA). The UK Met Office Radar data are kindly provided by the Nimrod System. NCAS British Atmospheric Data Centre.

6 References

Barnett C., J.Hossell, M.Perry, C.Procter and G.Hughes, G, A handbook of climate trends across Scotland. In SNIFFER project CC03, Scotland and Northern Ireland Forum for Environmental Research, 62, 2006.

Gleeson, E., Whelan, E., and Hanley, J.: Met ÃL'ireann high resolution reanalysis for Ireland, Adv. Sci. Res., 14, 49-61, doi:10.5194/asr-14-49-2017, 2017.

Graham, E., Climate Changes in the Hebrides, Stornoway Gazette, 2012.

Guerova, G., E. Brockmann, J. Quiby, F. Schubiger and C.H. Matzler, Validation of NWP mesoscale models with Swiss GPS network AGNES. Journal of Applied Meteorology, 42(1), 2003

Hou A.Y., R.K. Kakar, S. Neeck, A.A. Azarbarzin, C.D. Kummerow, M. Kojima, R. Oki, K. Nakamura and T. Iguchi, The Global Precipitation Measurement Mission, Bulletin of the American Meteorological Society, 95(5), 2014.

Jenkins G.J., M.C. Perry and M.J. Prior, The climate of the United Kingdom and recent trends. Met Office Hadley Centre, Exeter, UK, 2008.

Met Office, 1 km Resolution UK Composite Rainfall Data from the Met Office Nimrod System. NCAS British Atmospheric Data Centre, 2003.

Whelan, E., E. Gleeson, and J. Hanley: An evaluation of MÃL'RA, a high resolution mesoscale regional reanalysis. J. Appl. Meteor. Climatol., In press, https://doi.org/10.1175/JAMC-D-17-0354.1, 2018.

Wind-solar correlations and wind ramping events in reanalysis datasets over Ireland

Seánie Griffin[1], Conor Sweeney[1], and Frank McDermott[1]

[1]University College Dublin

1 Introduction

This study examines some uses of reanalysis datasets for analysing aspects of weather which are relevant for renewable energy in Ireland. Firstly, the skill of MÉRA (Glesson et al., 2017; Whelan et al., 2018) at representing observed daily mean 10 m wind speed is compared to two global reanalyses (ERA-Interim and MERRA-2).Combining wind and solar power production has the potential to reduce the overall variability of renewable energy generation. The statistical relationship between daily mean 10 m wind speed and daily total global shortwave radiation (SW) is analysed using Pearson's correlation coefficient. The correlation values calculated using reanalysis data are compared to observed values. Temporal variability of wind speeds has a large impact on wind power production. The ability of the respective reanalyses to replicate observed wind speed variability is investigated. This analysis is performed for different time periods (1-hour, 3-hour and 12-hour ramping).

All analysis is performed across a common validation period of 1982-2007 and the nearest grid point in each reanalysis is used to compare to observations.

2 Results

10 m Wind Speed

The accuracy of the 10 m wind speed is assessed using skill scores such as: mean error (ME), root mean square error (RMSE) and anomaly correlation coefficient (ACC). This analysis is performed for each of the three reanalyses.

The ME and RMSE for daily mean 10 m wind speed at seven Irish synoptic stations are presented in Figure 1. A positive bias is generally apparent at inland stations in MÉRA and at all stations for the global reanalyses (ERA-Interim and MERRA-2). MÉRA generally performs the best; it has the lowest ME and RMSE at five of the seven stations studied. MÉRA also has the best ACC scores at all seven stations (not shown). A large negative bias is apparent at Malin Head for MÉRA. Meanwhile large positive biases exist in ERA-Interim for Dublin and Valentia. These are most likely attributed to land/sea discrepancies.

Wind-Solar Correlation

Monthly wind-solar correlation values for each dataset are shown in Figure 2. These are averaged across the same seven stations shown in Figure 1. The correlation values calculated using reanalysis data tend to be further

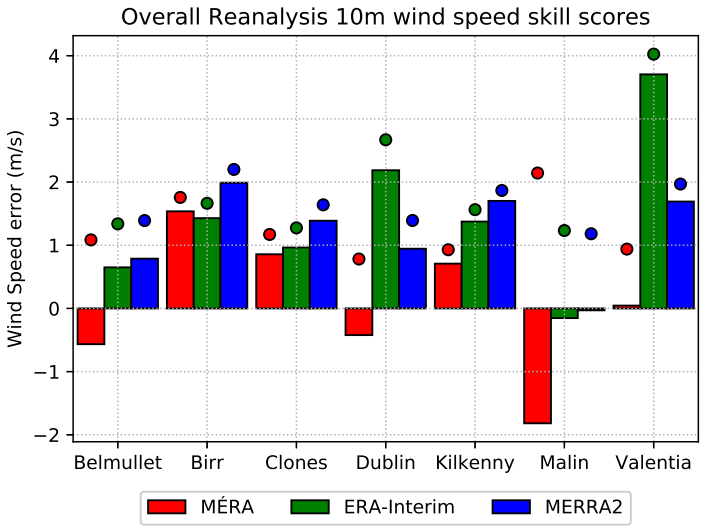

Figure 1: Skill scores (ME (bars) and RMSE (dots)) for daily mean 10 m wind speed at each station for MÉRA (red), ERA-Interim (green) and MERRA-2 (blue).

from zero than observations, indicating that they tend to overestimate the strength of the inverse relationship between wind speed and shortwave radiation. MERRA-2 moves closer to observations in the second half of the year (Fig. 2), but in general none of the reanalyses outperform the rest when considering all of the stations. This overestimation may need to be considered if reanalysis data are used to assess a site for combined wind and solar power generation.

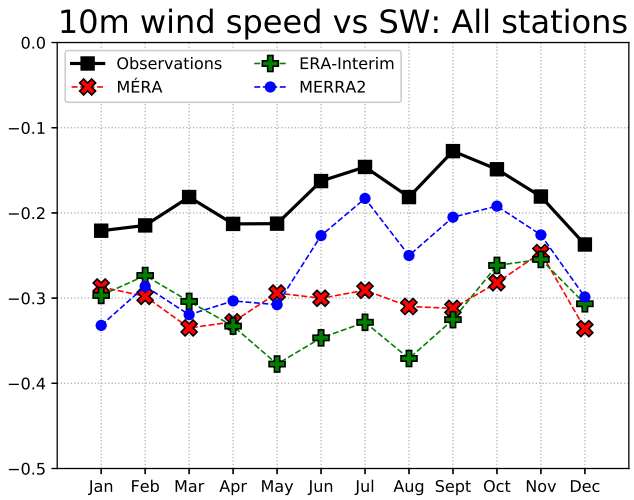

Figure 2: Monthly Pearson's correlation values between daily mean 10 m wind speed and daily total SW averaged for all seven stations. Observations (black), MÉRA (red), ERA-Interim (green) and MERRA-2 (blue)

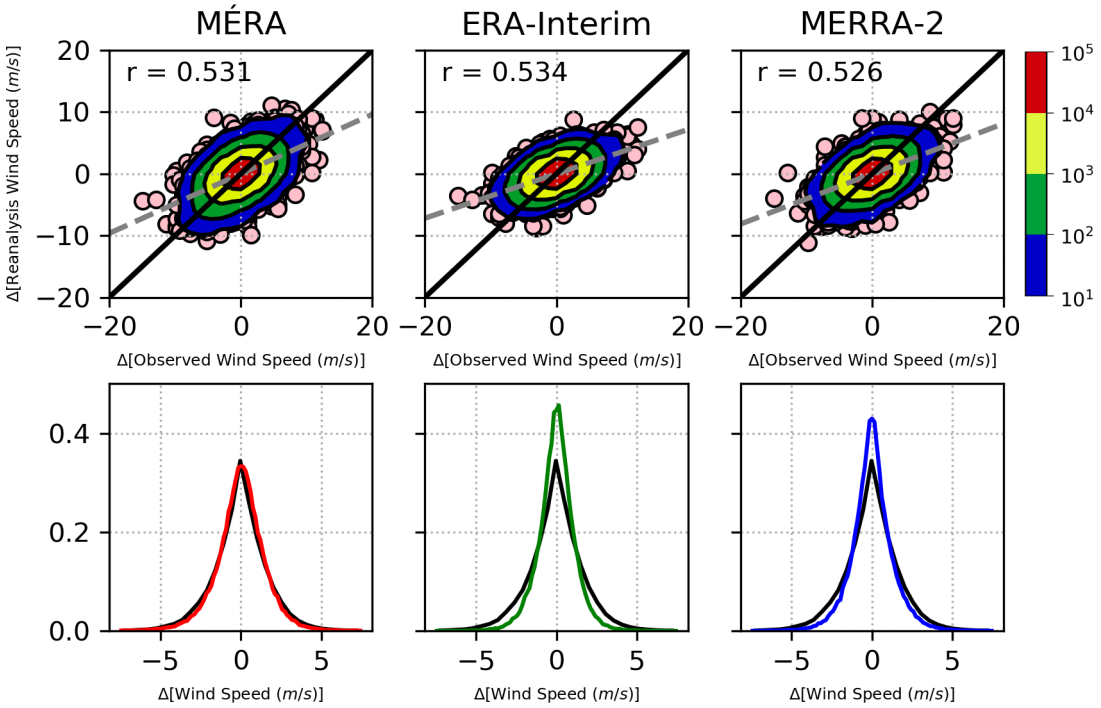

Figure 3: Ramping of 10 m wind speed over 3 hours at Kilkenny for MÉRA (left column), ERA-Interim (centre) and MERRA-2 (right column). The top row are contoured scatter plots of reanalysis ramps vs observed ramps, with best-fit line (dashed grey). The bottom row are histograms of 3 hour wind ramps for MÉRA(red), ERA-Interim (green), MERRA-2 (blue) and observations (black).

10 m Wind Speed Ramping

Temporal changes in wind power over a certain time horizon are referred to as wind ramping events. In this study, ramping of 10 m wind speed is examined at the seven synoptic stations shown in Figure 1. The results for 3 hour ramping at Kilkenny are presented in Figure 3 and Table 1. This is the shortest time period where all three reanalyses can be compared (ERA-Interim data are only available at 3-hourly resolution). In terms of point verification, all three reanalyses appear to struggle to match specific ramping events present in observations. This is indicated by the slope of best-fit lines being different from unity and low Pearson correlation (r) values in the scatter plots in Figure 3. These were similar to previous findings in Cannon et al. 2015.

The histograms in Figure 3 are used to assess the ability of the reanalyses to replicate the observed climatological distribution of wind ramping. MÉRA agrees best with the observations. Both global reanalyses tend to over predict small changes in wind speed and do not produce enough large ramp events. This is also illustrated when analysing the statistics shown in Table 1. The standard deviation and 5^{th} and 95^{th} percentiles of MÉRA are closer to the observed values than the two global reanalyses. The poor performance of global reanalyses for ramping over short time periods was also found in (Cradden et al. 2017) for the MERRA-2 reanalysis.

When the analysis is repeated for hourly ramping events, comparing MÉRA and MERRA-2, similar results are found. The MÉRA histogram again agrees best with the observations, with MERRA-2 exhibiting a thin-tailed distribution which underestimates extreme ramps. For studying wind ramping, MÉRA appears to add the greatest value when examining the climatology of ramping events over short time periods (e.g. ≤ 6 hours).

Table 1: The standard deviation (σ^2), 5^{th} (P05) and 95^{th} (P95) percentiles of 3 hour ramping events of 10 m wind speed at Kilkenny.

	Observations	MÉRA	ERA-Interim	MERRA-2
σ^2	1.691	1.538	1.141	1.314
P05	-2.572	-2.533	-1.90	-2.091
P95	2.572	2.395	1.813	2.178

3 Summary

- MÉRA performs best for 10 m wind speed at the majority of stations.
- All reanalyses tend to overestimate the strength of the inverse relationship between 10 m wind speed and shortwave radiation.
- MÉRA outperforms global reanalyses at capturing the temporal variability of 10 m wind speed over shorter time periods.

4 References

Cannon, D. J., D. J. Brayshaw, J. Methven, P. J. Coker, and D. Lenaghan: Using reanalysis data to quantify extreme wind power generation statistics: A 33 year case study in Great Britain. Renewable Energy 75: 767-778, 2015.

Cradden, Lucy C., Frank McDermott, Laura Zubiate, Conor Sweeney, and Mark O'Malley: A 34-year simulation of wind generation potential for Ireland and the impact of large-scale atmospheric pressure patterns. Renewable energy 106: 165-176, 2017.

Gleeson, E., Whelan, E., and Hanley, J.: Met Éireann high resolution reanalysis for Ireland, Adv. Sci. Res., 14, 49-61, doi:10.5194/asr-14-49-2017, 2017.

Whelan, E., E. Gleeson, and J. Hanley: An evaluation of MÉRA, a high resolution mesoscale regional reanalysis. J. Appl. Meteor. Climatol., In press, https://doi.org/10.1175/JAMC-D-17-0354.1, 2018.

Analysing Energy Demand and Weather in Ireland

Laura Cooke[1] and Conor Sweeney[1]

[1]University College Dublin

1 Introduction

The renewable energy sector in Ireland continues to grow as we strive towards reduced emissions targets. However, due to the irregular nature of weather, the sector faces challenges in producing enough energy when demand is high, or curtailing energy production when demand is low. Understanding the relationship between weather and energy demand is an important step towards improving the balance between power supply and demand at these key times. The purpose of this study is to introduce a model that can be used to investigate the relationship between the variability of energy demand and weather in Ireland.

2 All Ireland Electricity Demand Profile

All Ireland daily electricity demand data from January 2011 to December 2016 was obtained from the Single Energy Market Operator (SEMO). Figure 1 (left) shows this total demand profile, which can be broken into its low frequency and high frequency components. The low frequency component can be described as the combination of an annual trend and seasonal trend. Demand changes on an annual basis due to a variety of factors including climatic differences, Gross Domestic Product (GDP), electricity prices, technology evolution and societal changes. Seasonal variability of demand is driven by the cyclic changes in temperature and daylight hours throughout the year. The high frequency component of demand is driven by weather changes, day of the week and public holidays. Typically less electricity is consumed on weekends and public holidays.

Following Cradden and McDermott (2018) the low frequency component of demand can be represented by a second order Fourier Series y fitted to the daily demand data January 2011 - December 2016:

$$y = \overline{y} + a_1 \cos(\omega t) + b_1 \sin(\omega t) + a_2 \cos(2\omega t) + b_2 \sin(2\omega t),$$

where $\omega = \frac{2\pi}{365}$, $\overline{y}$ is a rolling 365-day mean and a_1, b_1, a_2, b_2 are Fourier coefficients. This Fourier fit is shown in Figure 1 (left). Subtracting the Fourier fit, y, from the total demand profile gives the high frequency component of demand, see in Figure 1 (right). This will be referred to as the residual demand and used to study the weather-driven component of the electricity demand.

3 Extreme Demand Profiles

The upper 90th percentile ($\geq 90\%$) and lower 10th percentile ($\leq 10\%$) of residual demand are used here to represent high and low extreme residual demand events respectively. The yearly and monthly profiles of extreme residual demand events (not shown) highlight the influence of public holidays on demand with a large

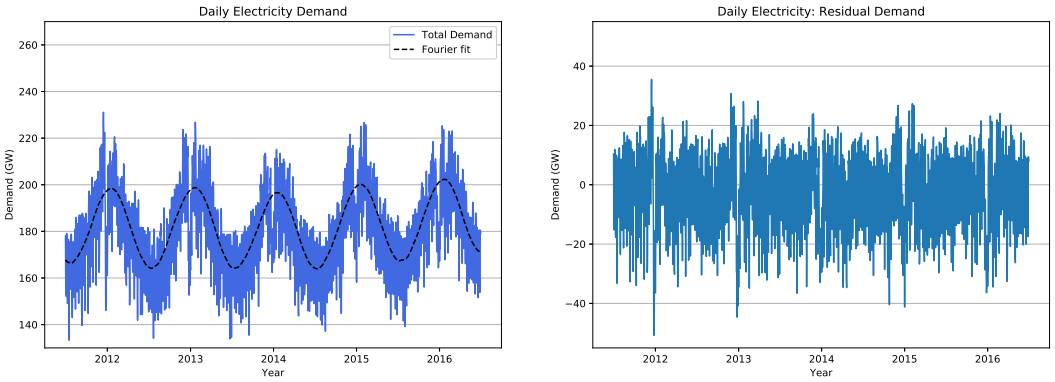

Figure 1: Left: Total daily electricity demand (–) and the Fourier Series fit representing the low frequency component of demand (- -). Right: Residual daily electricity demand, representing the high frequency component of demand.

number of extreme low residual demand days in December, presumably due to the Christmas break. While the extreme high residual demand days are most frequent in winter months and in 2011 and 2016, indicating the influence of weather on demand (winter 2011 was particularly cold).

4 Residual Demand Model

Multi-Variate Regression Model

Residual demand can be modelled by a multi-variate linear regression model similar to that used by Cradden and McDermott (2018), based on models by Taylor and Buizza (2003) and Bloomfield et al (2016).

The regression formula is given by:

$$\mathbf{D_R} = a\mathbf{T_e} + b{\mathbf{T_e}}^2 + c\mathbf{Cloud} + d\mathbf{Wind} + e\mathbf{Day} + f\mathbf{Hol} + g\mathbf{Xmas} + \epsilon,$$

where $\mathbf{D_R}$ is residual demand, $\mathbf{T_e}$ is effective temperature, $\mathbf{Cloud}$ is the cloud amount, $\mathbf{Wind}$ is wind speed, $\mathbf{Day}$ is a number representing day of the week, $\mathbf{Hol}$ is a true/false variable representing a public holiday, $\mathbf{Xmas}$ is a true/false variable representing the Christmas period (23^{rd} December - 4^{th} January), ϵ represents the model error and a, b, c, d, e, f, g are the model constants.

Effective temperature represents the tendency for demand to lag actual temperature changes, also effective temperature squared is included to capture the typically non-linear relationship between temperature and demand. Effective temperature is defined:

$$\mathbf{T_e}(t_n) = \frac{1}{2}\mathbf{T}(t_n) + \frac{1}{2}\mathbf{T}(t_{n-1}),$$

where t_n represents the n^{th} time step (day), and t_{n-1} the previous time step (day).

The true/false variables $\mathbf{Hol}$ and $\mathbf{Xmas}$, have a value of 1 when true and 0 when false. The $\mathbf{Day}$ variable is actually represented by five true/false variables representing mid-week days Tuesday/Wednesday/Thursday (since these days tend to have similar demand profiles) and individual days Monday, Friday, Saturday and Sunday.

$$e\mathbf{Day} = e_1\mathbf{Mon} + e_2\mathbf{MidWeek} + e_3\mathbf{Fri} + e_4\mathbf{Sat} + e_5\mathbf{Sun}.$$

Each of the five **Day** variables have a value of 1 when true and 0 when false.

With a focus on extreme demand events, the model was trained for winter. Using daily average weather observations at Dublin Airport on winter days between December 2011 and February 2016, the model was trained using a non-linear least squares method. Dublin observations were chosen to represent the highest density population centre in Ireland. The model obtained an R^2 value of 0.89 implying that it captures Irish daily demand profiles well. One month of the model fit (January 2016) is shown in Figure 2 (top).

Weather Driven Component of Demand

Once the regression model has been trained, the **Day**, **Hol** and **Xmas** variables can be removed to form a new model for weather-driven demand,

$$\mathbf{D_{weather}} \sim \mathbf{D_R} - e\mathbf{Day} - f\mathbf{Hol} - g\mathbf{Xmas}.$$

Figure 2 (bottom) shows the modelled weather-driven demand for one month (January 2016).

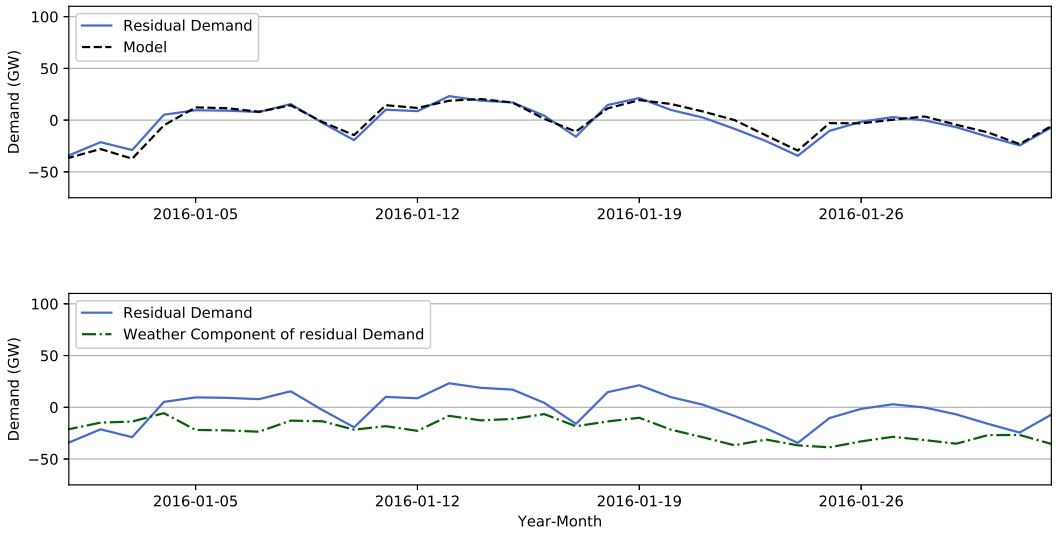

Figure 2: Residual daily demand for January 2016 (–) with the full multi-variate linear regression model (top – –) and the reduced model representing weather-driven demand (bottom –.–.).

5 MÉRA: Spatial Patterns of Weather on Extreme Demand Winter Days

This model for weather-driven demand was then used to study spatial patterns of extreme demand days in MÉRA (Glesson et. al., 2017; Whelan et al., 2018). The upper 90th percentile ($\geq$ 90%) and lower 10th percentile ($\leq$ 10%) of weather-driven demand days are used to represent extreme high and low weather-driven demand events, respectively. Figure 3 shows the 2 m temperature, 10 m wind speed and total cloud amount anomalies (from their climatology) averaged over extreme high and low weather-driven demand days. High weather-driven demand days are anomalously cold, with lighter than usual winds, and generally less cloudy than usual, while low weather-driven demand days are anomalously warm, with stronger winds and more cloud cover than usual. As a first approximation, these weather patterns can be likened to negative and positive winter NAO patterns for the high and low weather-driven demand cases, respectively.

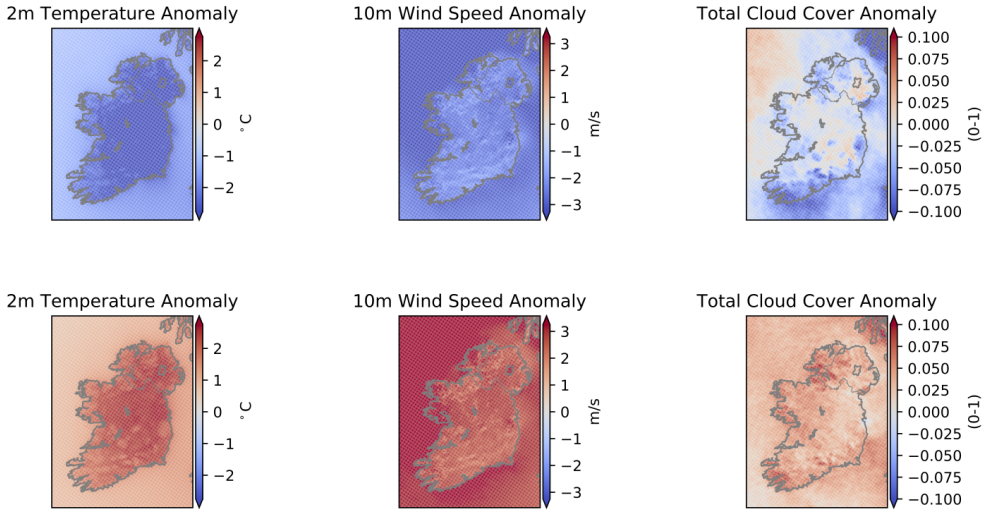

Figure 3: MÉRA 2 m temperature (left), 10 m wind speed (middle) and total cloud amount (right) anomalies averaged across extreme high (top) and low (bottom) weather-driven demand days in winter.

6 Conclusions and Future Work

This study implements and validates a regression model that can extract the weather-driven component of electricity demand. Further, the spatial patterns of extreme weather-driven demand days have been identified using MÉRA. This model combined with MÉRA has the potential to explore many interesting problems. Future work includes plans to improve the model by using MÉRA data to train it, specifically by weighting weather variables over large population centres. Furthermore, this model can be refined to represent hourly demand so that spatial patterns associated with extreme demand at key times of the day can be analysed. Finally, investigations into the demand response to extreme weather events will be carried out.

7 References

Bloomfield, H. C., D. J. Brayshaw, L. C. Shaffrey, P. J. Coker and H. E. Thornton, Quantifying the increasing sensitivity of power systems to climate variability, Environmental Research Letters, vol. 11, no. 12, 2016.

Cradden L. C. and F. McDermott, A weather regime characterisation of Irish wind generation and electricity demand in winters 2009-11, Environmental Research Letters, vol. 13, no. 5, 2018.

Gleeson, E., Whelan, E., and Hanley, J.: Met Éireann high resolution reanalysis for Ireland, Adv. Sci. Res., 14, 49-61, doi:10.5194/asr-14-49-2017, 2017.

SEMO: Single Electricity Market Operator, General Market Data: Daily Actual Load, *www.sem-o.com/MarketData/Pages/DynamicReports.aspx*, last checked: April 2018.

Taylor, J. W. and R. Buizza, Using weather ensemble predictions in electricity demand forecasting, International Journal of Forecasting, vol. 19, no. 1, 2003.

Whelan, E., E. Gleeson, and J. Hanley: An evaluation of MÉRA, a high resolution mesoscale regional reanalysis. J. Appl. Meteor. Climatol., In press, https://doi.org/10.1175/JAMC-D-17-0354.1, 2018.

An evaluation of MÉRA's representation of wind and solar variability associated with large-scale atmospheric pressure anomalies patterns

João Correia[1], Frank McDermott[1], Conor Sweeney[1]
[1] University College Dublin

1 Introduction

The continued addition of renewable energy sources (e.g. wind and solar) to the existing electricity grids will require a much better understanding of the natural spatiotemporal variability of atmospheric conditions. This in turn requires reliable gridded reanalysis products with good spatial and temporal coverage.

Here, we use Met Éireann's high-resolution reanalysis gridded dataset, MÉRA (Gleeson et al, 2017; Whelan et al, 2018), to analyse the links between atmospheric circulation patterns such as the North Atlantic Oscillation (NAO), the East Atlantic (EA) and Scandinavian (SCAND) patterns, for both wind speeds and incident shortwave (SW) radiation, in Ireland and the UK. For brevity, we restrict the results here to the NAO. We have performed the same analysis using the previously published lower resolution gridded datasets (e.g. MERRA2 and ERA-interim) to assess the advantages of MÉRA's higher resolution. Finally, we use MÉRA to assess the co-variability of the winter season wind and solar resources, and how these are linked to the NAO. All analyses were performed for the winter season (DJF), for the common period of 1982-2008, which is covered by the reanalysis and observational datasets used. The final section of the paper is restricted to considering MÉRA data only and this spans the longer period 1982-2016.

2 Large-scale pressure anomaly patterns

Teleconnection patterns are persistent, recurring large-scale patterns of atmospheric pressure and circulation anomalies. Some of these patterns have been linked with the low-frequency variability of various meteorological parameters in Europe, including parameters relevant to energy production (e.g. wind speed, rainfall, cloudiness surface incoming solar radiation) and energy demand (e.g. temperature). These patterns, having a stochastic nature over time, oscillate between positive and negative phases, with each associated with different atmospheric conditions. In the last few years, an increasing number of studies have related the seasonal and inter-annual variability of renewable power production and energy demand to some of these climate patterns and successfully explain why a given year or season was more/less (e.g.) windy than the average local conditions or why energy demand was higher/lower. These types of links between climate variability and renewable energy resources need to be assessed further and better understood as the share of wind and solar energy increases.

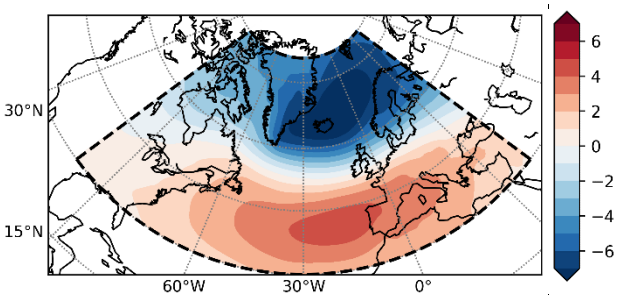

Figure 1: Spatial structure of the NAO teleconnection pattern. Scale reflects the SLP anomalies associated with each pattern. Patterns were derived from the ERA-interim reanalysis.

3 Results

Correlation maps: NAO-SW radiation

Pearson correlation scores between winter SW radiation and the NAO index were computed (Figure 2). Across both Ireland and the UK, a zonal gradient in the correlation scores is evident. In most of the western sectors of both islands, the surface incoming SW radiation varies negatively with the NAO index (anomalously high SW radiation in winters with a low NAO index), but that relationship weakens, loses significance and even changes sign (in the east UK mainland) zonally across the islands. The gradient is more noticeably captured by MÉRA (upper and lower right-hand plots below) and is also noticeable in the observational record (lower left-hand plot).

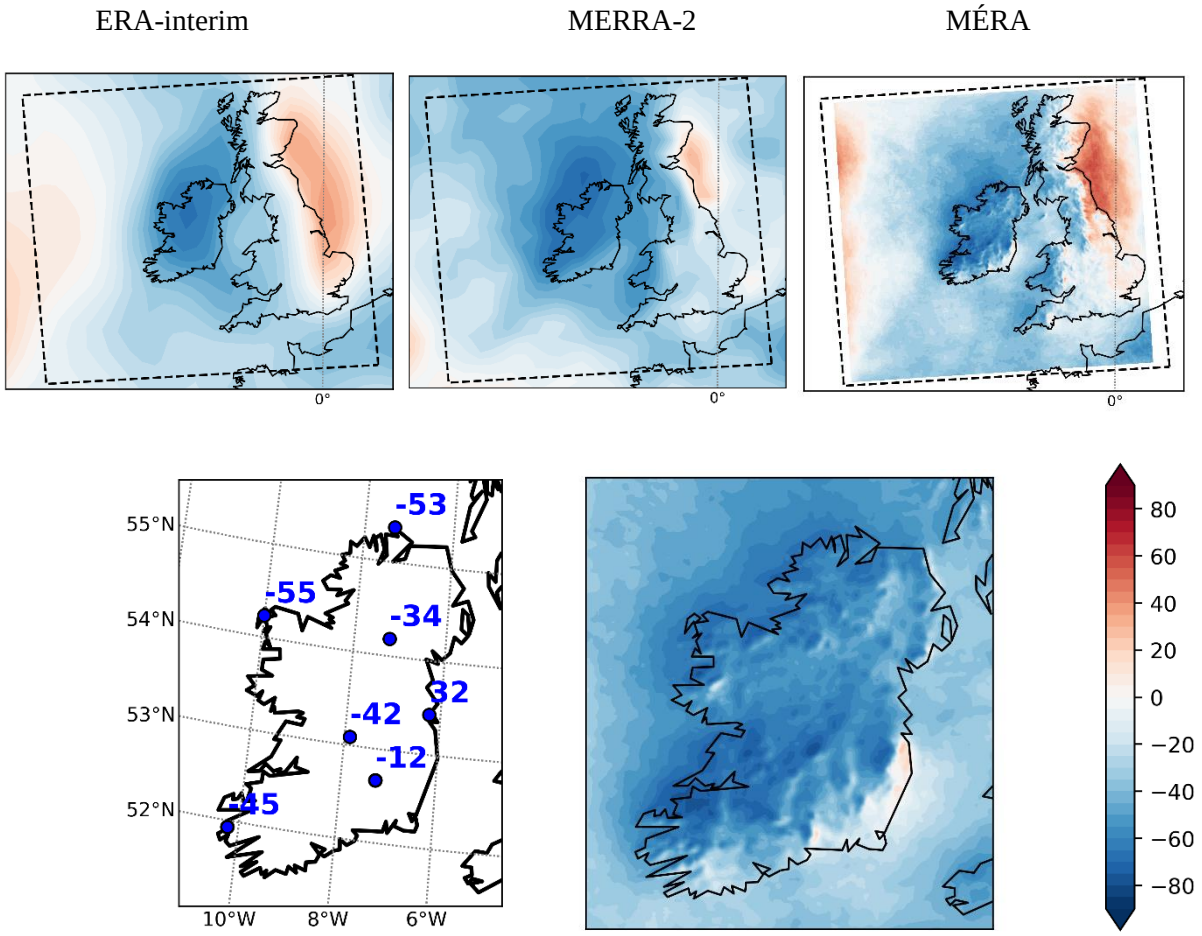

Figure 2: Pearson correlation scores (R x 100) between winter (DJF) SW radiation and the NAO index, for the period 1982-2008. The upper correlation maps show the scores obtained using the global horizontal SW radiation from the reanalysis datasets. The lower left-hand plot shows the scores obtained using weather station SW radiation observations. The lower right-hand plot is a close-up zoom of the upper right-hand plot (MÉRA).

Correlation maps: NAO-wind speed (h = 10 m)

Figure 3 represents the same analysis as Figure 2 but for wind speeds instead of incident SW radiation. A predominantly positive relationship between wind variability and the NAO was known for this geographical domain. However, the MÉRA dataset (upper and lower right) shows much greater detail,

including orographic effects on wind speed that are not captured by the two coarser resolution reanalysis products.

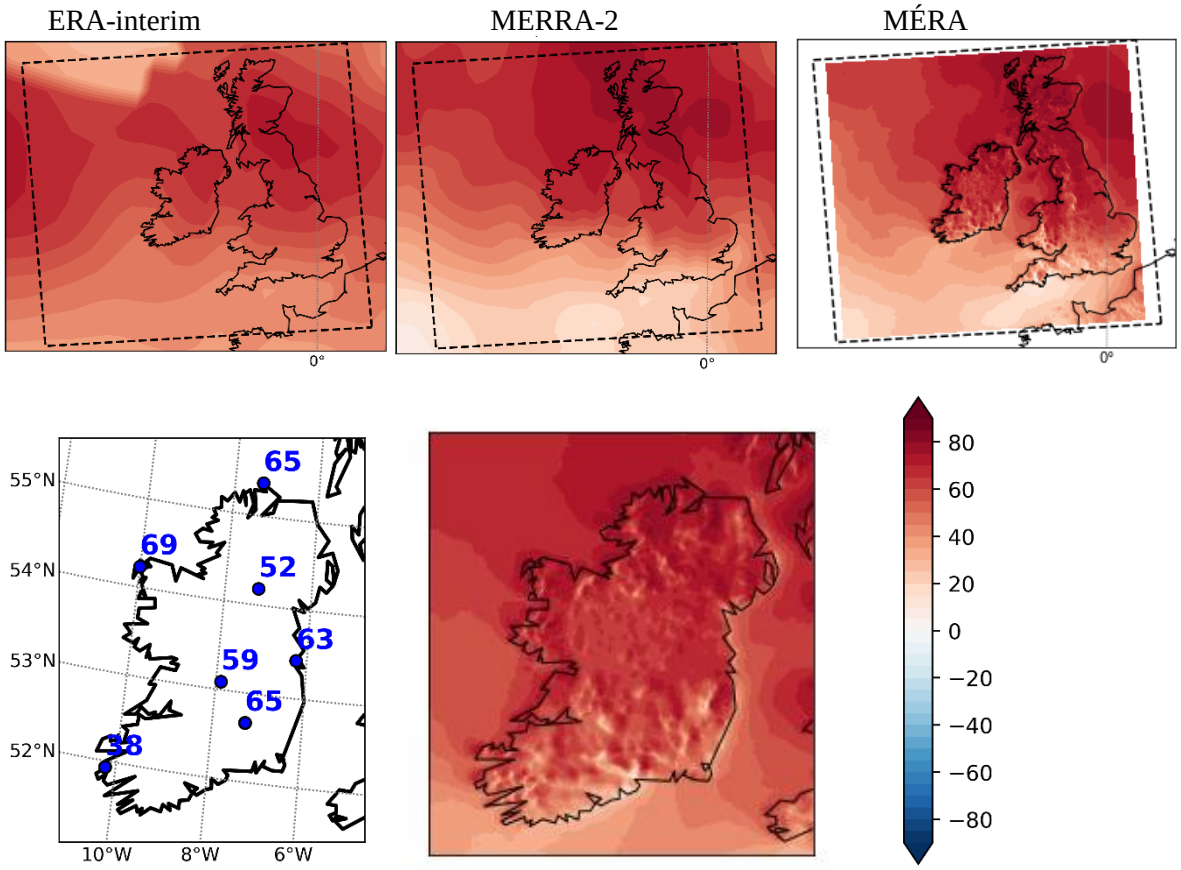

Figure 3: Pearson correlation scores (R x 100) between winter (DJF) 10 m metre wind speeds and the NAO index, for the period of 1982-2008. The upper correlation maps illustrate the scores obtained using wind speeds from the three reanalysis products. The lower left-hand plot shows the scores obtained using wind speed observations from meteorological stations. The lower right-hand plot is a close-up zoom of the top right plot (MÉRA) for the island of Ireland.

Correlation maps: Wind-solar relationships according to NAO phase

In Figure 4 below, the right-hand plot is a correlation map showing the relationship between the winter wind speeds and SW radiation. In most western parts of Ireland and the UK the incident SW radiation decreases as the average seasonal wind speed increases. In the southeast of Ireland, there appears to be no significant relationship between SW radiation and wind speeds.

For the island of Ireland, using every MÉRA grid point, we have plotted (left) the wind and solar anomalies for every winter season of the period 1982-2016 and have colour coded each data point according to the NAO phase of the winter that it represents. Although there is some overlap between anomalies (i.e. different winters and therefore NAO phases) it is clear that for most of Ireland, a positive (negative) NAO is associated with positive (negative) wind speed anomalies and negative (positive) incident SW radiation anomalies.

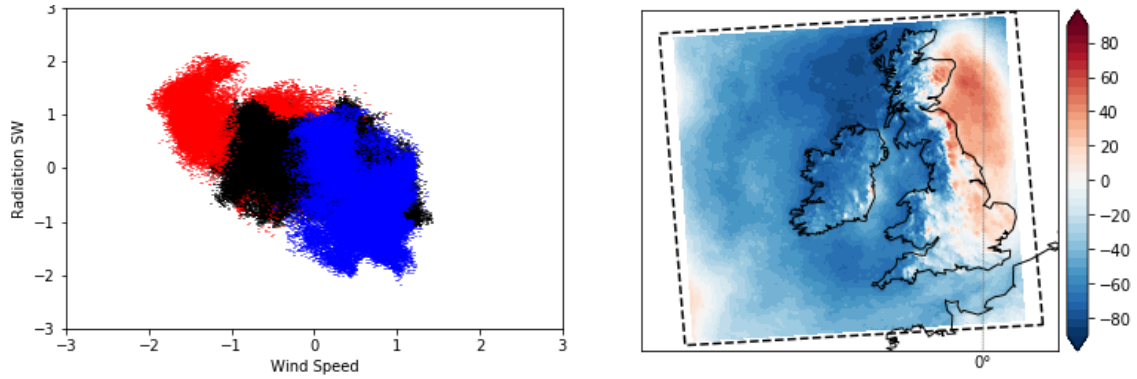

Figure 4: (Left) Wind speed and SW radiation normalised anomalies for every grid point of the island of Ireland. The anomalies are coloured according to the NAO phase – red (blue) refers to anomalies occurring in the negative (positive) phase of the pattern. Black refers to a weak/neutral NAO phase. (Right) Pearson's correlation score between wind speed (at a height of 100 meters) and SW radiation. Both plots cover the 1982-2016 period.

4 Summary

- General agreement between all three reanalysis datasets on the impact of large scale pressure patterns on winter wind speed and SW radiation (results shown here are only for the NAO).
    - As expected, the high resolution MÉRA reanalysis product offers a much more detailed assessment and allows orographic effects to be detected.
- Significant impact of the NAO on both winter wind speeds and incident SW radiation.
- Some degree of anti-correlation between wind and solar resources in Ireland and the UK, with a west to east change in the strength and sign of the correlation.

5 References

Colantuono, Giuseppe, Yimin Wang, Edward Hanna and. Robert Erdélyi. Signature of the North Atlantic Oscillation on British solar radiation availability and PV potential: the winter zonal seesaw. Solar Energy 107 (2014): 210-219.

Cradden, Lucy C., Frank McDermott, Laura Zubiate, Conor Sweeney, and Mark O'Malley. A 34-year simulation of wind generation potential for Ireland and the impact of large-scale atmospheric pressure patterns. Renewable energy 106 (2017): 165-176.

Gleeson, E., Whelan, E., and Hanley, J.: Met Éireann high resolution reanalysis for Ireland, Adv. Sci. Res., 14, 49–61, doi:10.5194/asr-14-49-2017, 2017.

Whelan, E., E. Gleeson, and J. Hanley: An evaluation of MÉRA, a high resolution mesoscale regional reanalysis. J. Appl. Meteor. Climatol., In press, https://doi.org/10.1175/JAMC-D-17-0354.1, 2018.

Wind energy production backcasts based on a high-resolution reanalysis dataset

Samuel Liu[1], Lucía Hermida González[2], Aoife M. Foley[3], and Paul G. Leahy[1,2]

[1]School of Engineering, University College Cork, Ireland
[2]Environmental Research Institute, University College Cork, Ireland
[3]School of Aeronautical and Mechanical Engineering, Queens University Belfast, Belfast, Northern Ireland

1 Introduction

The power outputs of renewable energy sources, such as wind, are variable in response to changing weather conditions. Forecasts of wind generation are therefore useful in order to help system operators schedule and dispatch generators in order to balance supply and demand at all times, to help energy traders predict supply and price movements on electricity markets, and to assist wind farm owners to schedule maintenance outages to minimise loss of output [Foley et al., 2012, Mc Garrigle and Leahy, 2015].

In recent years, as the proportion of total generation from variable, non-synchronous renewable energy sources, such as wind and solar photovoltaics, has increased. As a result, many new applications are emerging tha require accurate wind energy forecasts. For example, the increase in the penetration of renewable energy sources in many systems has led to electricity market reforms, including penalties for producing over or under the scheduled quantities. New hybrid wind-storage power plants have been deployed; the owners of these assets have to make decisions on when to store energy and when to release energy when trading on futures markets. The elimination of payments to renewable generators for energy curtailed for operational reasons by system operators is a further motivation for more accurate forecasting of wind generation.

Numerical weather prediction reanalysis data have been widely used in wind energy studies. Examples include large-scale wind resource analysis [Pryor et al., 2006] and wind energy backcast simulations for electricity market integration studies. The success of such studies is highly dependent on the accuracy of the datasets used. The relatively coarse horizontal spatial resolution of many reanalysis datasets, such as ERA-Interim (c. 80 km), limits their usefulness in such studies. The advent of high-resolution, regional datasets, such as Met Éireann's MÉRA reanalysis [Gleeson et al., 2017, Whelan et al., 2018], allows for more detailed backcasts to be developed, with corresponding improvements in accuracy. The 2.5 km horizontal resolution of MÉRA, in combination with its previously-reported low bias compared to ERA-Interim 10 m wind speeds, makes it ideal for wind energy production estimation, because the spatial resolution is sufficient to resolve some terrain effects.

The increase in accuracy of numerical weather prediction (NWP) forecasts in recent years has led to a significant performance improvement in wind energy forecasting. The HARMONIE-AROME configuration of the shared ALADIN-HIRLAM system used by Met Éireann and other meteorological agencies runs with a grid spacing of 2.5 km, which allows for resolution of some localised influences on wind speeds which would not be possible in models with coarser spatial resolution. As the resolution of MÉRA is the same as that of the operational HARMONIE-AROME model used by Met Éireann, the results of this MÉRA backcasting exercise should provide insight into the capability of the operational model to resolve local effects on wind power generation.

In this study, we investigate the accuracy of wind energy production backcasts for a wind farm location in Ireland derived from MÉRA data. The results of various bias correction schemes are introduced, with the overall results showing good prediction accuracy even when relatively simple corrections, such as the Kalman filter, are applied.

2 Data and methods

The chosen wind farm site is on relatively flat terrain in the midlands of Ireland, and has a site mean wind speed of 7.7 $\mathrm{m\,s^{-1}}$ at 100 m above ground according to the Sustainable Energy Authority of Ireland's wind atlas[1]. There are eighteen 2,000 kW turbines on the site, each with a hub height of 95 m. Wind speed measurements from a meteorological mast on the site were supplied by the site operator.

Data processing

We use horizontal wind speed components at 10 m and 100 m levels from the MÉRA (Met Éireann ReAnalysis) dataset as inputs to the wind energy forecast model. Interpolation of wind data, u, at the four nearest grid cells, (1,1; 1,2; 2,1; 2,2), to the location of the wind farm, u_{loc}, was achieved by using a least squares method (Eqn. 1).

$$u_{loc} = a\,u_{1,1} + b\,u_{1,2} + c\,u_{2,1} + d\,u_{2,2} \tag{1}$$

10 m wind speeds were initially provided by Met Éireann, and these were extrapolated to turbine hub height using the power law and an assumed shear coefficient of α=0.143. When 100 m wind speeds became available for download, these were then used as inputs to the wind energy forecast. Prediction intervals of 3 h and 24 h were selected from the MÉRA dataset. Wind speeds at hub height were then transformed to wind generation time series by applying a speed-to-power transformation based on the turbine manufacturer's power curve. The power curve was scaled to match the wind farm's maximum export capacity. No attempt was made to incorporate the effects of turbine wake interactions or outages.

Historic generation output values at 30-minute time resolution were obtained from the Single Electricity Market Operator's website [2]. Local measurements of wind speed at 95 m height and ten-minute time resolution were also provided by the wind farm operator for 2016.

Data corrections

Several approaches were used reduce the bias and other errors in the wind energy forecast model. A persistence correction was applied in the first instance. Its purpose was to provide a lagging bias correction, and a simple benchmark correction against which to measure other more sophisticated methods.

The next level of forecast correction was the application of threshold corrections to the persistence-corrected wind energy time series. Because the persistence correction is a lagging correction, it may lead to physically unrealistic output values (e.g. power values that exceed the capacity of the wind farm, or negative values). These were removed by employing a simple thresholding approach; i.e. where values exceed the maximum export capacity of the wind farm, they are set to the maximum export capacity, and where values are negative they are assigned a value of zero.

The Kalman filter, a more sophisticated forecast correction method, was then employed. The Kalman filter is an optimal estimator for linear dynamical systems [Faragher, 2012]. "Optimal" in this case implies that the least squares prediction error is minimised. That makes it ideal for use in applications such as position estimation from noisy data, and bias correction of wind forecasts [Louka et al., 2008, Sibuet Watters and Leahy, 2011,

[1] SEAI wind atlas, http://maps.seai.ie/wind/

[2] Single Electricity Market Operator Dynamic Reporting Tool, http://www.sem-o.com/marketdata/Pages/dynamicreports.aspx

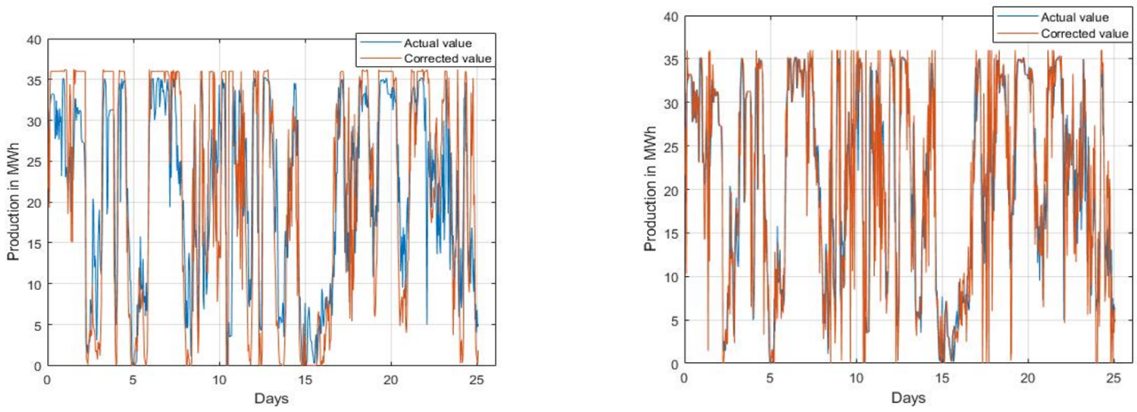

Figure 1: Wind generation backcast derived from (a) "raw" MÉRA data (red) and (b) persistence-corrected MÉRA data with threshold corrections applied (red) for February 2014. Actual generation values are shown in blue.

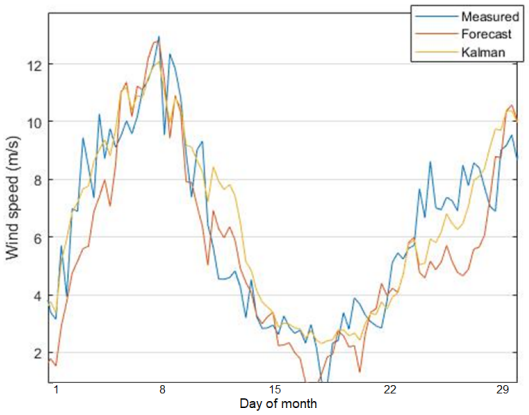

Figure 2: Wind speed backcast derived from MÉRA data with Kalman filter correction for January 2016.

Cassola and Burlando, 2012]. In this case, the Kalman filter was used to derive a state vector $\hat{x}(t)$ to minimise the bias in the forecast time series.

Several error metrics were used to evaluate the performance of the overall system, including: mean error (ME or bias), normalised mean absolute error (NMAE) and root mean squared error (RMSE).

3 Results

Sample time series of uncorrected, bias-corrected and threshold-corrected wind generation backcasts are presented in Figs. 1 and 2. The Kalman filter was applied to both wind power and wind speed time series, with better performance observed on wind speed time series (Fig. 2). The Kalman-corrected wind speed time series were subsequently transformed to wind power.

A sensitivity analysis was carried out in order to determine the most sensitive parameters in the wind generation model. Four factors contributing to the overall uncertainty of the output were selected and adjusted, and the corresponding changes in the output accuracy were calcluated. The four factors were: shutdown of three

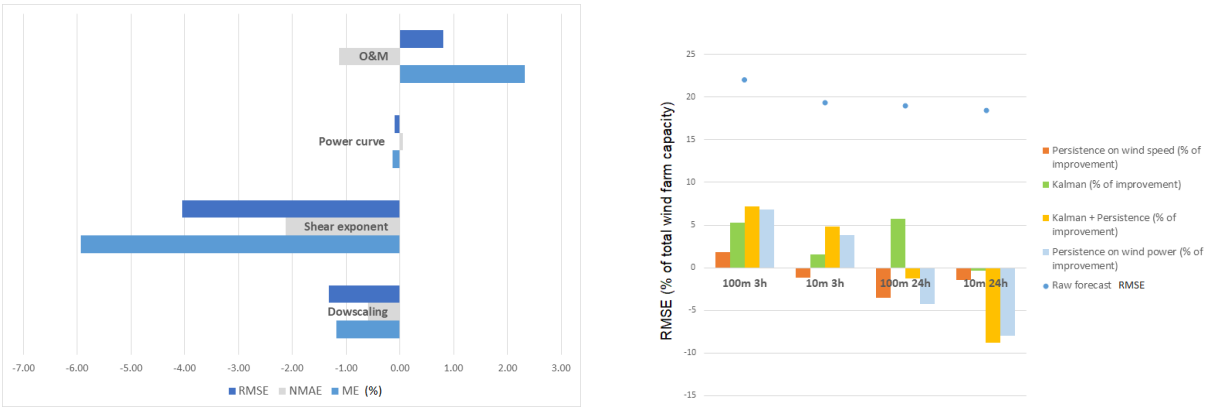

(a) (b)

Figure 3: (a) Sensitivity analysis of the wind generation forecast (% errors) to model parameters. (b) Improvements in RMSE over "raw" MÉRA-based forecasts (blue circles) for different prediction intervals (3 h & 24 h) of 10 m and 100 m wind speeds.

turbines ("O&M"), derating of the power curve by 1% ("power curve"), variation in the value of shear exponent (α) for vertical extrapolation by 0.07, and the choice of spatial interpolation (single nearest neighbour versus weighted combination of four nearest neighbours) to the target wind farm location ("downscaling"). The resulting changes in RMSE, NMAE and ME are presented in Fig. 3a. The results show that the shear exponent for vertical extrapolation was the most sensitive factor examined in the analysis.

4 Discussion and Conclusions

Using the uncorrected MÉRA wind speeds for wind generation backcasting produces good results despite the simplicity of the wind energy forecast model. Fig. 1a shows that, even without any corrections to the raw MÉRA data, a simplistic speed-to-power conversion produces realistic values for wind farm generation output. This underlines the high accuracy of wind speeds in the MÉRA dataset. Application of relatively simple corrections (persistence and threshold cutoffs, Fig. 1b) further improves the model performance, with a visible reduction in bias (Fig. 3b and Table 1).

Table 1: Root mean squared error (MWh) of wind energy backcasts derived from uncorrected ("raw") MÉRA wind speeds and from various corrections applied to MÉRA data, for 10 m and 100 m wind speeds and 3 h and 24 h prediction intervals.

	Raw	Persistence	Persistence + Thresholds	Kalman
100 m, T+3 h	7.94	5.48	5.20	6.04
10 m, T+3 h	6.99	5.60	5.33	6.44
100 m, T+24 h	6.84	8.38	6.88	4.78
10 m, T+24 h	6.64	9.52	7.25	6.76

In general, the model performance is consistent across all error parameters used in this study, and in particular for the mean error. Forecasts for the T+3 h prediction interval are only slightly more accurate than for the T+24 h prediction interval. The Kalman-corrected forecasts based on 10 m wind speed data produce lower errors, especially much lower bias, than those based on the 100 m wind speeds. As expected, the Kalman filter is efficient at eliminating systematic biases such as those introduced by vertical extrapolation of wind speeds. This is also consistent with the results of the initial parameter sensitivity analysis. The performance of the various forecast corrections are summarised in Fig. 3b and Table 1.

The Kalman filter applied to MÉRA data produces good results for each error metric and in particular reduces the systematic bias. The advantage of the Kalman filter is also seen for the longer prediction interval (T+24 h; Table 1) where it has the lowest RMSE of the four approaches. Noise at longer prediction intervals is more likely to approach a Gaussian distribution which is one of the assumptions underlying the Kalman filter. Thus, the Kalman filter efficiency depends more on the nature of the forecast errors than the overall accuracy of the backcast. Furthermore, access to measured wind speed data is key for good performance of the Kalman filter performance as these assist the model update step used for bias correction.

The results of this wind energy generation forecasting exercise demonstrate that the accuracy of wind speeds from high resolution reanalysis datasets such as MÉRA should make such datasets extremely valuable in wind resource assessment. Further work will concentrate on more sophisticated corrections such as the extended Kalman filter which should further reduce the errors in wind generation forecasts derived from MÉRA wind speeds.

Acknowledgements

This material is partially based upon research supported by the Irish Environment Protection Agency (Grant Award No. 2016-W-MS-23) for the project "Tools for Climate Change Attribution of Extreme Weather Events in Ireland (ClimAtt)". The authors acknowledge Met Éireann for providing the MÉRA reanalysis data and advice, and the operator of the wind farm for providing site meteorological data.

References

[Cassola and Burlando, 2012] Cassola, F. and Burlando, M. (2012). Wind speed and wind energy forecast through Kalman filtering of numerical weather prediction model output. *Applied Energy*, 99:154 – 166.

[Faragher, 2012] Faragher, R. (2012). Understanding the basis of the Kalman filter via a simple and intuitive derivation. *IEEE Signal Processing Magazine*, 29(5):128–132.

[Foley et al., 2012] Foley, A. M., Leahy, P. G., Marvuglia, A., and McKeogh, E. J. (2012). Current methods and advances in forecasting of wind power generation. *Renewable Energy*, 37(1):1–8.

[Gleeson et al., 2017] Gleeson, E., Whelan, E., and Hanley, J. (2017). Met Éireann high resolution reanalysis for Ireland. *Advances in Science & Research Open Access Proceedings*, 14:49–61.

[Louka et al., 2008] Louka, P., Galanis, G., Siebert, N., Kariniotakis, G., Katsafados, P., Pytharoulis, I., and Kallos, G. (2008). Improvements in wind speed forecasts for wind power prediction purposes using Kalman filtering. *Journal of Wind Engineering and Industrial Aerodynamics*, 96(12):2348 – 2362.

[Mc Garrigle and Leahy, 2015] Mc Garrigle, E. V. and Leahy, P. G. (2015). Quantifying the value of improved wind energy forecasts in a pool-based electricity market. *Renewable Energy*, 80:517–524.

[Pryor et al., 2006] Pryor, S. C., Barthelmie, R. J., and Schoof, J. T. (2006). Inter-annual variability of wind indices across Europe. *Wind Energy*, 9(1-2):27–38.

[Sibuet Watters and Leahy, 2011] Sibuet Watters, C. and Leahy, P. (2011). Downscaling numerical weather predictions of wind speeds using the Kalman filter. In *Proceedings of the 10th International Conference on Environment and Electrical Engineering*, Rome.

[Whelan et al., 2018] Whelan, E., Gleeson, E., and Hanley, J. (2018). An Evaluation of MÉRA, a High-Resolution Mesoscale Regional Reanalysis. *Journal of Applied Meteorology and Climatology*, 57(9):2179–2196.

Shortwave Radiation in Reanalyses: Skill Scores and Spatial Patterns

Eadaoin Doddy[1], Conor Sweeney[1], and Frank McDermott[1]

[1]University College Dublin

1 Introduction

Unlike conventional power stations that can operate anywhere continuously to meet demand, renewable energy technology is dependent on local weather conditions which can be highly variable. Therefore, spatial analysis of shortwave (SW) radiation is essential in planning of viable locations for solar energy generation. Reanalysis data can be used in regions where observations are sparse, such as SW radiation observations in Ireland. The accuracy of reanalysis data must be assessed before use. If an element of the error is systematic, then there is potential to reduce this error through post-processing techniques.

SW radiation is the main parameter used in the generation of solar energy. It is produced by the sun but can be reflected by clouds (~24%) or absorbed by aerosols (~17%) before it reaches the surface. This makes SW radiation variable on high-resolution temporal and spatial scales. Here the daily accumulated SW radiation is compared to seven Irish weather observing stations for the period 1982-2007. The spatial pattern of SW radiation around Ireland is also compared to satellite data. The common weather patterns associated with large error events are also investigated.

2 Skill Scores

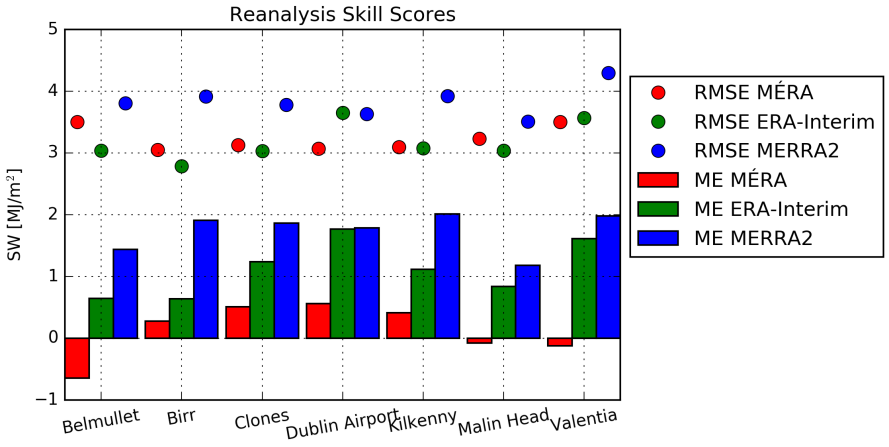

Figure 1: Mean Error (bars) and RMSE (dots) in SW radiation for seven weather observing stations in Ireland (1982-2007) for three reanalysis datasets; MÉRA (red), ERA-Interim (green) and MERRA-2 (blue).

In Ireland typical winter values of daily SW radiation are approximately 3 MJ/m^2 and summer values are approximately 16 MJ/m^2. Standard skill scores including mean error (ME), root mean square error (RMSE), anomaly correlation coefficient (ACC) and Pearson's correlation are used to assess the accuracy of SW radiation estimated by three reanalyses - MÉRA, ERA-Interim and MERRA-2. The results are shown in Figure 1. MÉRA has the lowest ME at all stations. ERA-Interim values of RMSE are often the best, although are comparable with MÉRA at some stations. ERA-Interim and MERRA-2 overestimate SW radiation at all stations, which is consistent with previous studies (Zhang et al, 2016; Boilly and Wald, 2015). MÉRA also overestimates SW radiation except at Atlantic facing stations (Valentia, Belmullet and Malin Head) where there is a negative bias. This may be due to how the model expresses water content in the atmosphere column.

When skill scores are averaged over all 7 stations MÉRA has the best ME and ACC, while results are comparable with ERA-Interim for RMSE and Peason's correlation. High Pearson's correlation values (>0.9) show that all reanalyses capture the variability well.

3 Spatial Patterns

The SW radiation spatial patterns are shown in Figure 2. Satellite data is used as a refernce. There is a variation in the north-south direction which is expected as SW radiation varies with latitude. There is also an east-west variation which is highlighted by the contrast in SW radiation values over land and sea. SW radiation values are larger over the sea than over land. Previous studies often exclude SW radiation values over the sea. MÉRA performs best at representing the spatial pattern observed in the satellite data. ERA-Interim also does well in capturing this pattern, but the patterns are less pronounced in MERRA-2.

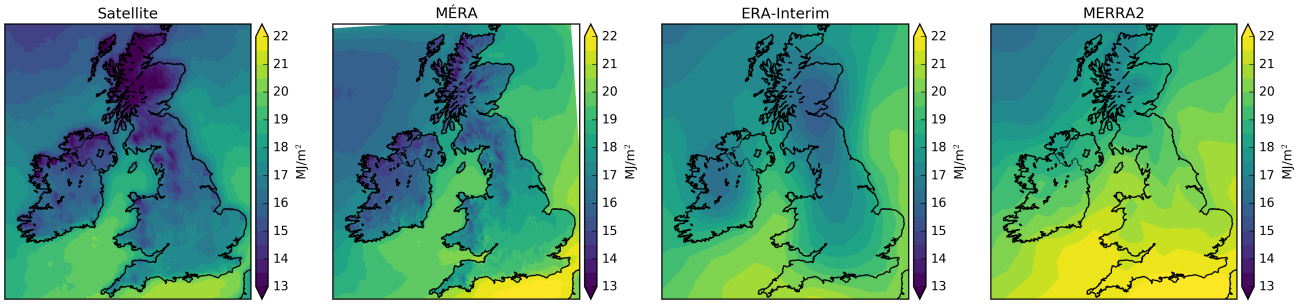

Figure 2: Spatial pattern of average summer total daily SW irradiance for Satellite, MÉRA, ERA-Interim and MERRA-2.

4 Post-processing

A linear-least squares post-processing technique shows improvement in skills scores (Figure 3). The largest improvements in ME and RMSE are found in the low-resolution reanalyses, which originally had the larger errors. ME is reduced to close to zero in all three reanalyses and at all stations. There is also a reduction in RMSE after post-processing, although the improvement is not as large as that of ME.

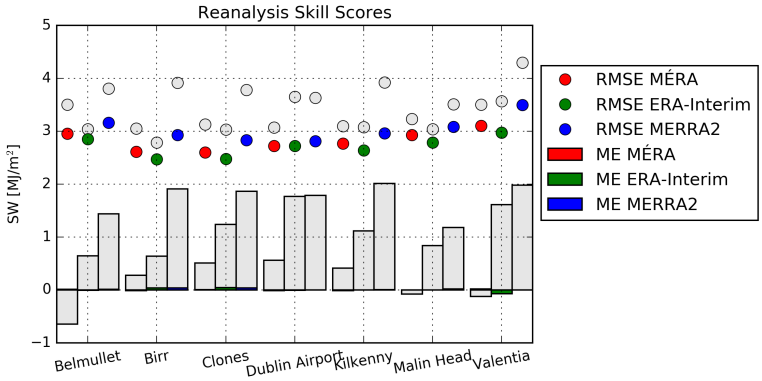

Figure 3: Mean Error (bars) and RMSE (dots) for the seven synoptic stations in Ireland for SW radiation (1982-2007) for the three reanalyses; MÉRA (red), ERA-Interim (green) and MERRA-2 (blue). The grey bars and dots in the background are the original values before post-processing, as shown in Figure 1, for comparison.

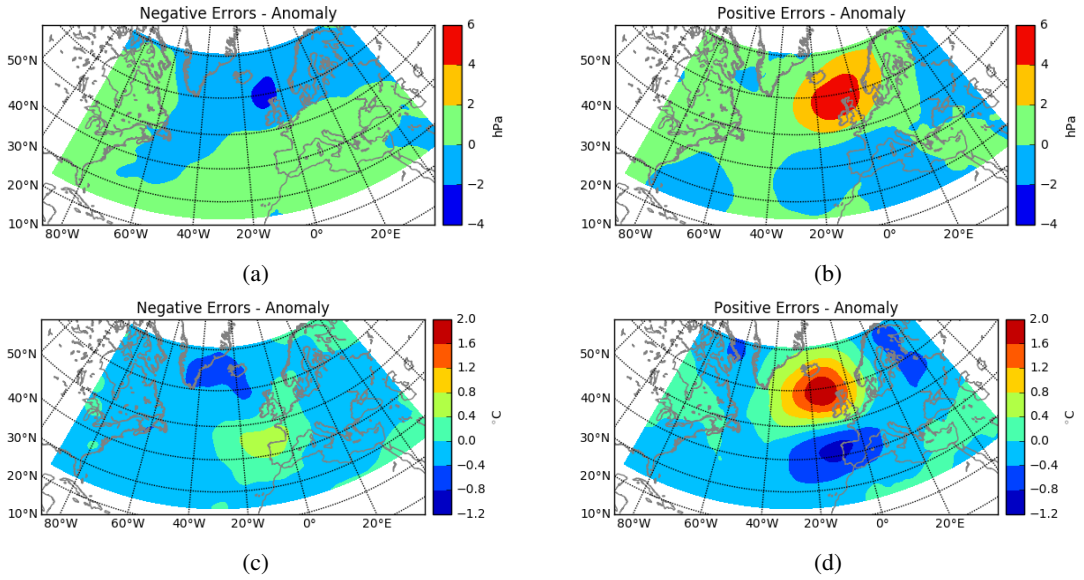

Figure 4: MSLP anomalies in ERA-Interim averaged over all large negative SW radiation error events and large positive SW radiation error events in MÉRA. Temperature at 500 hPa anomalies in ERA-Interim averaged over all large negative SW radiation error events and large positive SW radiation error events in MÉRA.

5 Large Error Events - Common Weather Patterns

Finally, we investigate if there are common weather patterns associated with days when large errors occur in SW irradiance. The 200 largest positive and negative error events for each station are selected. The model has large error events in the months from March to October inclusive, there are no large error events in winter. This is because SW irradiance values are relatively low in winter.

ERA-Interim data are used to examine the large-scale common weather patterns which occurred during these events. Initial analysis, as shown in Figure 4, suggests that mean sea level pressure (MSLP) shows a high positive anomaly compared to a 30-year climatology for positive error (model overestimates SW irradiance) events and a negative anomaly for negative error (model underestimates SW radiation) events. Simultaneously,

a positive anomaly is observed in temperature at 500 hPa to the north of Ireland while a negative anomaly is observed south of Ireland for positive error events. The reverse is observed with a weaker gradient for negative error events.

6 Summary

- MÉRA generally yields better skill scores.
- A simple post-processing technique reduces systematic errors in all reanalyses.
- MÉRA captures the spatial variability of SW irradiance best.
- Future work includes:
  - Principle component analysis (PCA) on weather patterns for large error events.
  - Novel adaptive spatial multivariate post-processing methods.

7 References

Boilley, A. and Wald, L., Comparison between meteorological re-analyses from ERA-Interim and MERRA and measurements of daily solar irradiation at surface, Renewable Energy, 75, 135-143, 2015.

Gleeson, E., Whelan, E., and Hanley, J.: Met Éireann high resolution reanalysis for Ireland, Adv. Sci. Res., 14, 49-61, doi:10.5194/asr-14-49-2017, 2017.

Whelan, E., E. Gleeson, and J. Hanley: An evaluation of MÉRA, a high resolution mesoscale regional reanalysis. J. Appl. Meteor. Climatol., In press, https://doi.org/10.1175/JAMC-D-17-0354.1, 2018.

Zhang, X., Liang, S. Wang, G., Yao, Y., Jiang, B. and Cheng, J., Evaluation of the reanalysis surface incident shortwave radiation products from NCEP, ECMWF, GSFC, and JMA using satellite and surface observations, Remote Sensing, 8, 225, 2016.

Extreme Wave Events of Winter 2013/2014 off the West Coast of Ireland

Jelena Janjić[1], Sarah Gallagher[1,2], and Frédéric Dias[1]

[1]MaREI Centre, University College Dublin
[2]Research, Environment and Applications Division, Met Éireann

1 Introduction

This study looks at extreme waves, defined as waves of larger than expected amplitude, in the waters off the west coast of Ireland. These extreme events can manifest as transitory waves of great height, or as prolonged sea states of great energy. The force of waves during these events can pose a threat to the effective and safe management of offshore operations. Though both manifestations of extreme waves bring more energy, Wave Energy Converters (WECs) are very sensitive to these situations, especially if they are deployed in unsheltered locations. An excess of such energy could be disastrous to a WEC, leading to fatal structural damage, component malfunction, mooring system failure and more. Therefore, the knowledge of extreme sea states or individual waves is essential for WEC design, deployment and operation. This study can be used also for decision-making regarding wind turbine accessibility, which is highly dependent on the wave period and atmospheric conditions. We are interested in the storm events of winter 2013/2014 off the west coast of Ireland which caused serious and widespread coastal damage and a record 23.4 m maximum individual wave height (significant wave height of over 15 m) at the M4 wave buoy off the coast of Donegal. A study by Matthews et al. (2014) showed that the winter of 2013/2014 was the stormiest in the last 143 years. This winter experienced beach changes (Masselink et al., 2016), severe hurricane strength winds, above average rainfall amounts and notable storm surges (Met Office: Winter storms: December, n.d.; Met Office: Winter storms: January, n.d.; Met Office: Winter 2013/14, n.d.; Met Éireann: December, n.d.; Met Éireann: January, n.d; Met Éireann: Winter, n.d.) causing a lot of coastal damage, transport disruption, inland flooding, felled trees, and power losses across the Atlantic coast of Europe and recorded human fatalities in Ireland and UK. We used the third generation WAVEWATCH III wave model (Tolman , 2014) version 4.18 in an unstructured formulation (Roland, 2008), and driven by MÉRA (Met Éireann ReAnalysis) 10 m winds (Gleeson et al., 2017; Whelan et al., 2018) and ERA-Interim directional wave spectra (Dee et al., 2011). The wave model has a high-resolution grid (up to 225 m resolution in the nearshore) with approximately 20000 nodes. The analysis of the winter storms of 2013/2014 includes maps and time-series of various wave parameters outputted hourly (wave energy flux, peak wave direction, and peak wave period). These wave parameters describe the wave characteristics which are important to wave energy conversion (average energy available for extraction, the direction of incoming waves, and wave frequency/period). The model results are validated against buoy data in order to provide a high quality, high-resolution hindcast of the wave events during winter 2013/2014.

2 Methodology

The bathymetry in Fig. 1 was generated using a Digital Elevation Model (DEM) for Ireland (Gallagher et al., 2014). The unstructured triangular grid (see Fig. 1) has a varying resolution of 10 km offshore to 225 m

nearshore (Gallagher et al., 2016). WAVEWATCH III is driven hourly with MÉRA 10 m wind forcing fields with a 2.5 km horizontal resolution and European Centre for Medium-Range Weather Forecasts (ECMWF) ERA-Interim 2–D wave spectra with a temporal resolution of 6 h in 10 points around the boundary of the model.

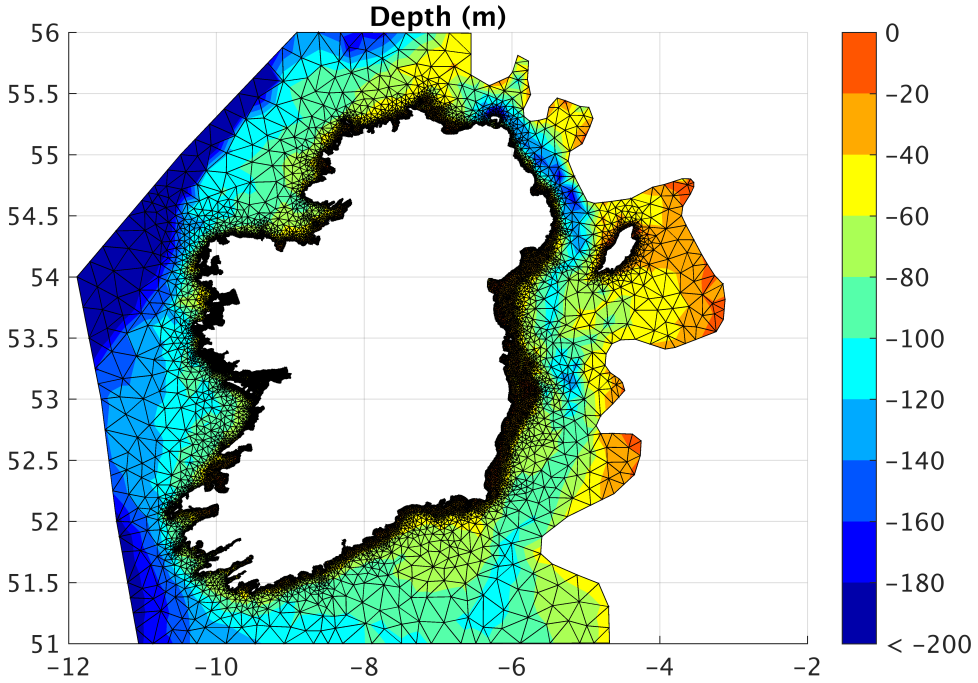

Figure 1: The WAVEWATCH III model unstructured grid and bathymetry (Gallagher et al., 2016).

For brevity, we chose to show two major storms in February 2014: (i) an unnamed storm on the 1st and (ii) the "Darwin" storm on the 12th. Each of these storms is described and discussed in detail in the Results sections below. We give an overview of the storms importance and weather and wave conditions on the day of the storm. We analyse time series of the significant wave height and maps of the significant wave height (H_s), peak wave period (T_p), and peak wave direction (D_p). We examine wind speeds and directions in three locations taken from The Unified Climate and Synoptic Observation Network (TUCSON): Malin Head, Mace Head, and Sherkin Island (only ones of most significance to the storms analysis have been shown). These are Automatic Weather Stations (AWS) which are part of Met Éireann's synoptic weather observation network. These stations were chosen for analysis because they are both close to the coastline and the wave measurement locations.

Table 1: Statistical parameters for H_s

Location name	CC	σ_A (m)	σ_B (m)	Bias (m)	Slope	SI	n
Kinsale	0.97	1.81	1.86	0.1	0.94	0.13	2151
Killard	0.94	1.92	2.21	0.09	0.82	0.17	1487
M4	0.95	1.68	2.27	0.32	0.82	0.15	821

3 Results

We validated the model by comparing it to the available buoy data in three locations: M4 Irish Weather Buoy Network buoy (55, –9.99) off the northwest coast, Killard off Co. Clare (52.774, –9.587), and Kinsale Energy

Gas Platform (51.37, –7.945)) off the south coast. In Fig. 2 we show the time series comparison at the Kinsale Energy Gas Platform. The values of the statistical parameters for H_s at different locations are summarised in Table 1. These parameters are defined as follows: Pearson correlation coefficient (CC), standard deviation of the model (σ_A) and measured value (σ_B), bias, slope, scatter index (SI), and number of records (n).

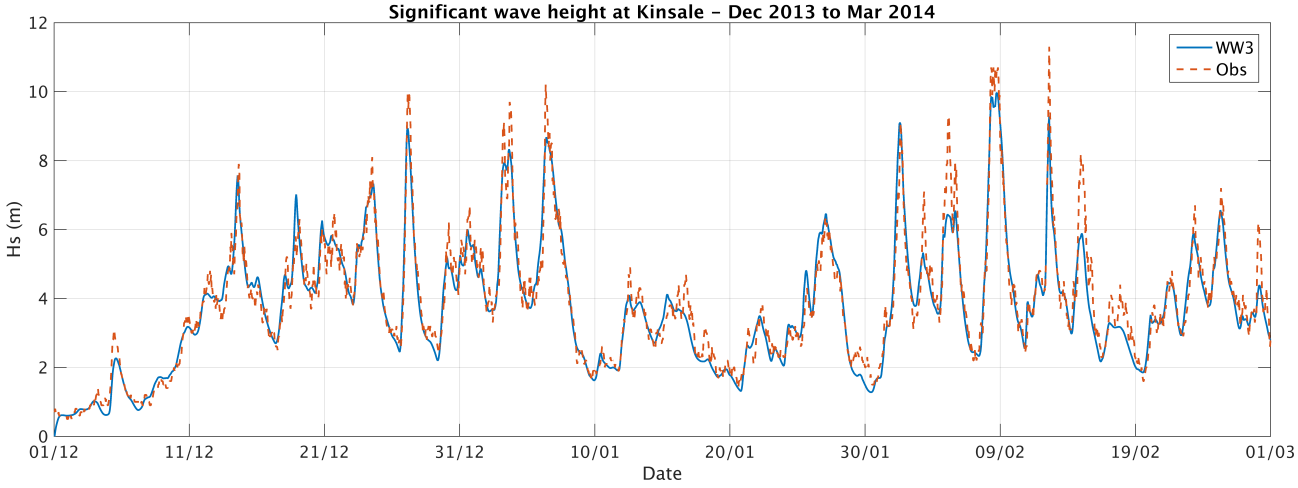

Figure 2: Timeseries of significant wave height from December 2013 to March 2014 comparing observations from the Kinsale Energy Gas Platform (51.37, –7.945) radar and modelled values.

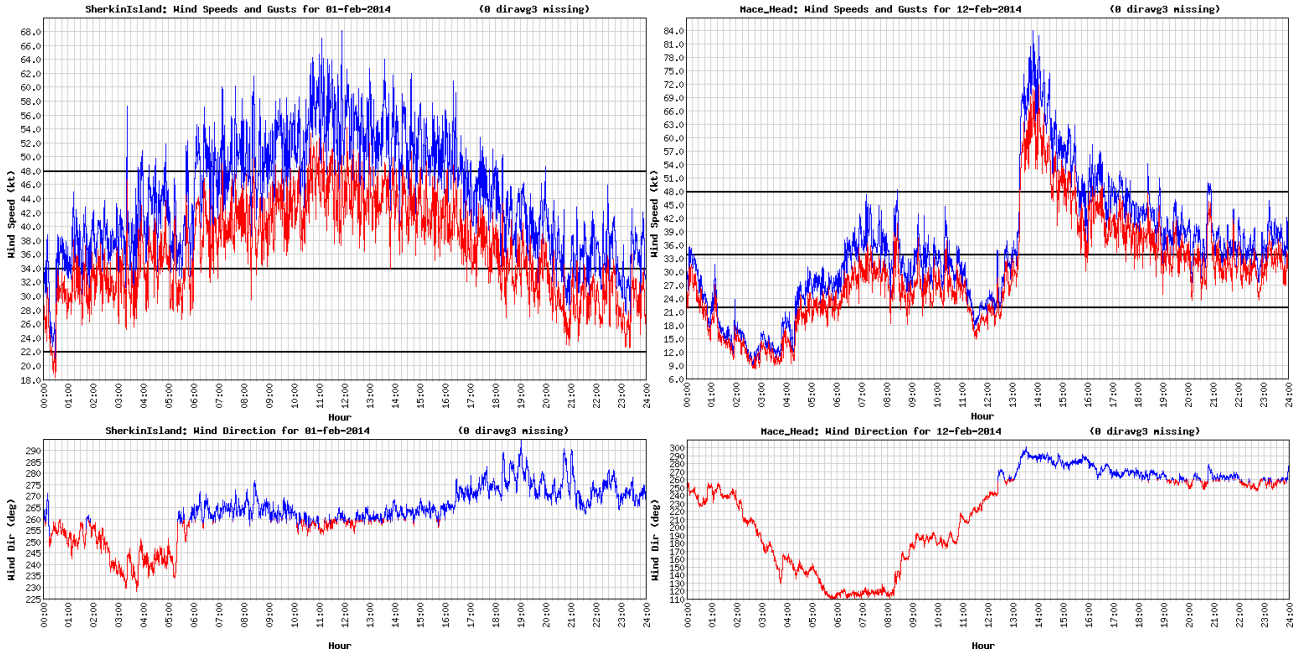

(a) Sherkin Island – 1st February 2014

(b) Mace Head – 12th February 2014

Figure 3: Observations from Met Éireann Synoptic (TUCSON) stations for wind speeds and gusts (kt) (top panels) and direction (°) (bottom panels). Top panels: Red = wind speed (kt); Blue = wind gust (kt). For context, horizontal lines show mean speed boundaries on the Beaufort scale. Force 6 "Strong breeze" (22 kt); Force 8 "Gale" (34 kt); and Force 10 "Storm" (48 kt). Note the different scales for wind speed.

For parameter definitions see Janjić et al. (2018). The model reproduced the extreme wave events well, only slightly underestimating the peak wave heights during the passing storms. The agreement could be improved by

feeding the model with hourly ECMWF operational archive 2-D wave spectra in more points on the boundary of the model.

The storm on the 1st of February is a result of a deep low pressure system of 955 hPa. This storm stands out from the rest of the February storms because of the coastal flooding and damage it caused across Ireland, particularly Co. Cork (O'Brien et al., 2018). The winds were strong gale or storm force with south to southwest direction (Met Éireann: February, n.d). Observations from Met Éireann Synoptic (TUCSON) stations at Sherkin Island (Fig. 3a) show that the mean wind speed reached values of 54 kt (100 km/h) and gust of 68 kt (126 km/h). A large rogue wave was recorded by the Killard Electricity Supply Board (ESB) buoy with a maximum wave height of 28.08 m in the H_s of 12.34 m sea state on the 1st Feb at 1100 UTC (O'Brien et al., 2018).

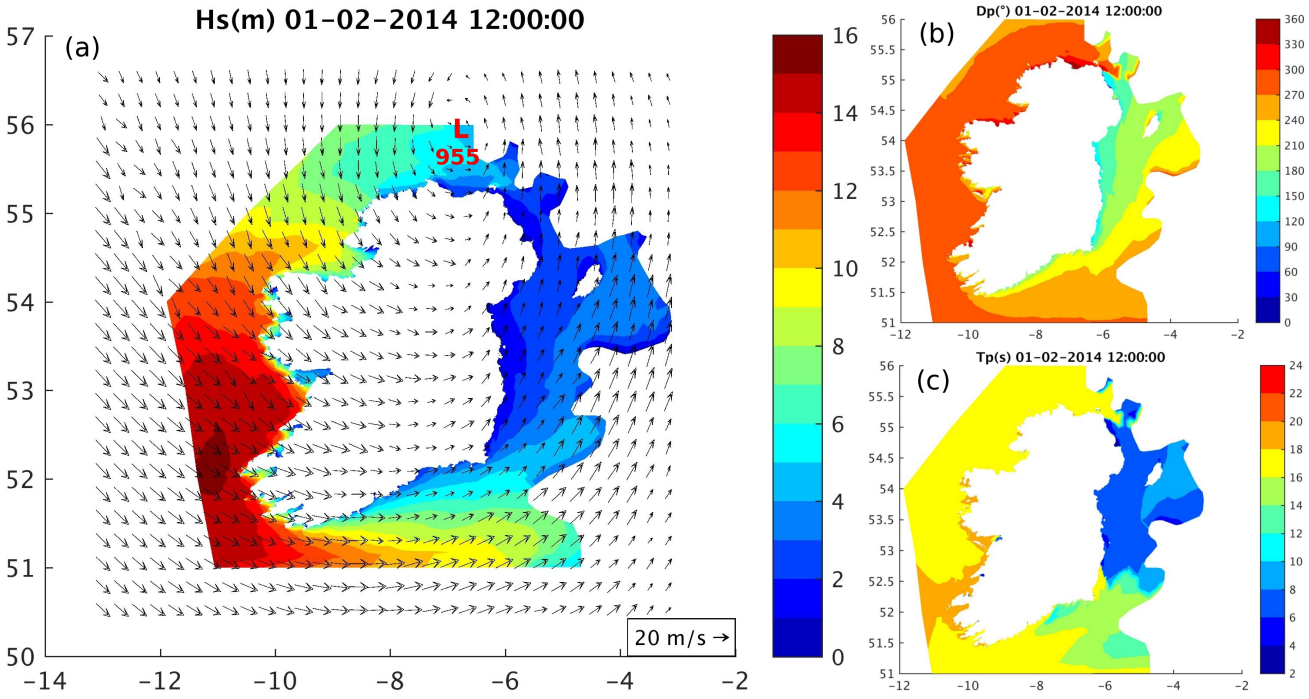

Figure 4: Maps of a) significant wave height (m) with vectors representing wind speed (m/s) and direction (°) and the center of the low pressure system "L" of 955 hPa, b) peak wave direction (°), and c) peak wave period (s) at 1200 UTC on the 1st of February 2014.

The Darwin storm, associated with a deep low pressure system of 955 hPa (see Fig. 5a) over Ireland, was the most severe storm of winter 2013/14. A maximum mean wind speed of 117 km/h was recorded at Mace Head (Fig. 3b) and maximum gusts of 156 km/h at Shannon Airport (hurricane force winds) which are the season's highest, with a south to southwest direction (Met Éireann: February, n.d). It is interesting to note that between 1300 UTC and 1400 UTC at Mace Head a significant jump in the wind speed and gust values was recorded indicating that the storm front was passing at this time over the station. The direction of the wind changed significantly in approximately 5 hours, again, indicating the passing of the storm. On the 12th of February the Kinsale Energy Gas Platform wave radar measured a maximum wave height of 25 meters (Mc Grath, 2015; O'Brien et al., 2018).

Although these two storms share similarities, such as the minimum sea level pressure value and strong winds, they were very different as well. The 1st February storm approached Ireland as an almost fully developed storm, slowly weakening from its peak reached in the early morning hours of the day (around 0200 UTC). The "Darwin" storm on the other hand experienced an explosive growth in Irish nearshore waters (around 0900 UTC) followed by fast abatement (Mc Grath, 2015). The 1st February storm covered a larger area than

the "Darwin" storm which was in comparison smaller, slightly stronger and very focused. Therefore, these differences are the reason behind the two different sea states that resulted from these storms.

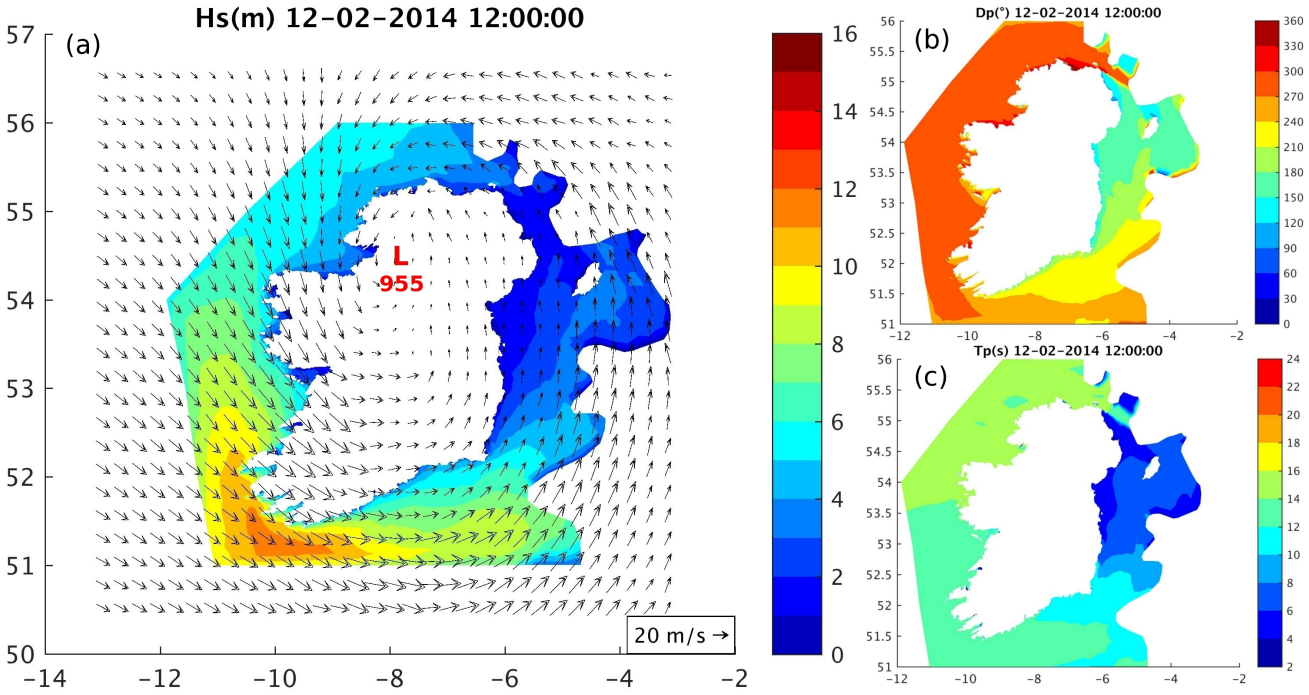

Figure 5: Maps of a) significant wave height (m) with vectors representing wind speed (m/s) and direction (°) and the center of the low pressure system "L" of 955 hPa, b) peak wave direction (°), and c) peak wave period (s) at 1200 UTC on the 12th of February 2014.

The maximum H_s of 15 m occurred at 1200 UTC on the 1st February with T_p 16–18 s and D_p of 270°–300° (northwest – oceanographic convention). The maximum H_s can be found to the right of the storm propagation where the strongest winds are (Fig. 4). We can see that the high energy sea state is widespread, which comes from the fact that this storm was a larger scale storm which was already developed as it propagated towards Ireland, creating large waves on the way. The direction of the most energetic waves corresponds to the direction of the strongest winds (Fig. 3a). The wave period indicates that the dominant waves (highest waves) are long swell.

The weather conditions on the 12th of February caused waves with a maximum H_s of 11.5 m, T_p of 12–16 s and D_p of 270°–300° (northwest – oceanographic convention). Again, area with the highest H_s matches the area with the strongest winds and this area is as expected very narrow and focused just as the area of strong winds is (Fig. 5). The direction of the strongest waves matches the direction of the winds. The wave period of the most energetic waves is lower when compared to the first storm, indicating that these may be closer to wind sea than swell, generated nearer to the coastline.

4 Conclusions

In order to reproduce the wave events of winter 2013/14, we used the WAVEWATCH III model forced with MÉRA 10 winds and ECMWF ERA-Interim 2-D wave spectra. We simulated December 2013, January, and February 2014 of this winter and we analysed two events on the 1st and 12th February. Keeping in mind that the model underestimates H_s when compared to measurements, the maximum H_s of 15 m was reached by the

model on the 1st of February at 1200 UTC. These two events show different atmospheric conditions resulting in different sea states that can be equally dangerous. We can have a highly widespread and energetic sea state, a more focused and unexpected energetic state, and among these sea states it is possible to even have rogue waves, highly energetic and unexpected waves. Phenomenal sea-states occurred off the west coast of Ireland during the winter of 2013/2014, and these extreme wave events need to be taken in account not only in the stage of WEC design, deployment, and operation but also to improve our understanding and forecasting of these extreme coastal hazards.

5 Acknowledgments

This work is supported by Science Foundation Ireland (SFI) through Marine Renewable Energy Ireland (MaREI), the SFI Centre for Marine Renewable Energy Research-(12/RC/2302). The authors want to thank the Irish Centre for High-End Computing (ICHEC) for the provision of computational facilities. The authors thank Met Éireann for providing the M4 and Kinsale Gas Energy Platform wave data, wind and gust data and the ESB for the Killard Waverider buoy data.

6 References

Dee, D. P., Uppala, S. M., Simmons, A. J., Berrisford, P., Poli, P., Kobayashi, S., Andrae, U., Balmaseda, M. A., Balsamo, G., Bauer, P., Bechtold, P., Beljaars, A. C. M., van de Berg, L., Bidlot, J., Bormann, N., Delsol, C., Dragani, R., Fuentes, M., Geer, A. J., Haimberger, L., Healy, S. B., Hersbach, H., Hólm, E. V., Isaksen, L., Kållberg, P., Köhler, M., Matricardi, M., McNally, A. P., Monge-Sanz, B. M., Morcrette, J.-J., Park, B.-K., Peubey, C., de Rosnay, P., Tavolato, C., Thépaut, J.-N., and Vitart, F.: The ERA-Interim reanalysis: configuration and performance of the data assimilation system, Q. J. Roy. Meteor. Soc., 137, 553–597, https://doi.org/10.1002/qj.828, 2011.

Gallagher, S., Tiron, R., and Dias, F.: A long-term nearshore wave hindcast for Ireland: Atlantic and Irish Sea coasts (1979–2012), Ocean Dynam., 64, 1163–1180, 2014.

Gallagher, S., Gleeson, E., Tiron, R., McGrath, R., and Dias, F.: The Nearshore Wind and Wave Energy Potential of Ireland: A High Resolution Assessment of Availability and Accessibility, Renew. Energ., 88, 494–516, https://doi.org/10.1016/j.renene.2015.11.010, 2016.

Gleeson, E., Whelan, E., and Hanley, J.: Met Éireann high resolution reanalysis for Ireland, Adv. Sci. Res., 14, 49–61, https://doi.org/10.5194/asr-14-49-2017, 2017.

Janjić, J., Gallagher, S., and Dias, F.: Case study of the winter 2013/2014 extreme wave events off the west coast of Ireland, Adv. Sci. Res., 15, 145-157, https://doi.org/10.5194/asr-15-145-2018, 2018.

Matthews, T. K. R., Murphy, C., Wilby, R. L., and Harrigan, S.: Stormiest winter on record for Ireland and UK, Nat. Clim. Change, 4, 738–740, https://doi.org/10.1038/nclimate2336, 2014.

Masselink, G., Castelle, B., Scott, T., Dodet, G., Suanez, S., Jackson, D. , and Floc'h, F.: Extreme wave activity during 2013/2014 winter and morphological impacts along the Atlantic coast of Europe, Geophys. Res. Lett., 43, 2135–2143, DOI: 10.1002/2015GL067492, 2016.

Mc Grath, R.: Impact of Storm Darwin on Ireland: description of the event and assessment of weather forecasts, Met Éireann, Technical Note No. 64, ISSN: 1393-905X, available at: https://www.met.ie/cms/assets/uploads/2017/08/2014StormDarwin-1.pdf, last access: 10 August 2018.

Met Éireann: Winter 2013/2014, available at: http://www.met.ie/climate-ireland/weather-events/WinterStorms13_14.pdf, last access: 13 August 2018.

Met Éireann: February 2014 Monthly Weather Bulletin No. 333, available at: https://www.met.ie/climate/past-weather-statements, last access: 13 August 2018.

Met Éireann: January 2014 Monthly Weather Bulletin No. 332, available at: https://www.met.ie/climate/past-weather-statements, last access: 13 August 2018.

Met Éireann: December 2013 Monthly Weather Bulletin No. 332, available at: https://www.met.ie/climate/past-weather-statements, last access: 13 August 2018.

Met Office: Winter 2013/14, available at: https://www.metoffice.gov.uk/climate/uk/summaries/2014/winter, last access: 14 Nov 2017a.

Met Office: Winter storms, January to February 2014, available at: https://www.metoffice.gov.uk/climate/uk/interesting/2014-janwind, last access: 8 Nov 2017b.

Met Office: Winter storms, December 2013 to January 2014, available at: https://www.metoffice.gov.uk/climate/uk/interesting/2013-decwind, last access: 8 Nov 2017c.

O'Brien, L., Renzi, E., Dudley, J. M., Clancy C., and Dias, F.: Catalogue of extreme wave events in Ireland: revised and updated for 14680 BP - 2017. Natural Hazards and Earth System Sciences, 18 (3), pp.729-758, 2018, DOI: 10.5194/nhess-18-729-2018.

Roland, A.: Development of WWM II: Spectral wave modelling on unstructured meshes, Institut für Wasserbau und Wasserwirtschaft, Technische Universität Darmstadt, 2008.

Tolman, H.: The WAVEWATCH III Development Group (2014), User Manual and System Documentation of WAVEWATCH III version 4.18, Tech. Note 316, NOAA/NWS/NCEP/MMAB, 2014, available at: http://polar.ncep.noaa.gov/waves/wavewatch/manual.v4.18.pdf, last access: 13 August 2018, 2014.

Whelan, E., E. Gleeson, and J. Hanley: An evaluation of MÉRA, a high resolution mesoscale regional reanalysis. J. Appl. Meteor. Climatol., In press, https://doi.org/10.1175/JAMC-D-17-0354.1, 2018.